A New Spatial Downscaling Method for Long-Term AVHRR NDVI by Multiscale Residual Convolutional Neural Network

Mengmeng Sun, Xiang Zhao, Jiacheng Zhao, Naijing Liu, Siqing Zhao, Yinkun Guo, Wenxi Shi, and Longping Si

***Abstract*—Monitoring vegetation dynamics is essential for ecological processes, environmental changes, and natural resource protection. Fine-scale representation of vegetation indices is necessary for regions with complex topography and high diversity species. However, the advanced very-high-resolution radiometer (AVHRR), which covers an extensive time range with high temporal resolution, does not provide normalized difference vegetation index (NDVI) data with sufficient spatial resolutions for a detailed analysis of vegetation changes. The moderate resolution imaging spectroradiometer (MODIS), which has a higher temporal and spatial resolution, has only been limited to the last few decades. To deal with these issues, we propose a multiscale residual convolutional neural network (MRCNN) that utilizes a multiscale structure with a residual convolutional neural network to combine MODIS NDVI and AVHRR NDVI data. The MRCNN algorithm improved mean absolute error (MAE) and root mean squared error (RMSE) by 0.026 and 0.032, respectively, resulting in a 64.38% improvement for MAE and 62.79% improvement for RMSE compared to AVHRR NDVI. It also increased the peak signal-to-noise ratio by 28.5% and the structural similarity index by 16.2%. The MRCNN method accurately captures the actual state of MODIS NDVI and consistently tracks changing trends in the vegetation index. It is exact in complex terrain and diverse vegetation areas. This method enhances the spatial resolution of AVHRR NDVI and significantly improves the accuracy of monitoring nationwide vegetation index changes over 30 years. The findings establish a solid scientific foundation for implementing ecological conservation measures and promoting sustainable vegetation growth.**

***Index Terms*—Advanced very-high-resolution radiometer (AVHRR) normalized difference vegetation index (NDVI), diverse features, multiscale structure, residual block.**

I. Introduction

THE normalized difference vegetation index (NDVI) is a significant metric utilized to characterize vegetation condition as well as its relationship with the natural environment or human activities (e.g., agricultural practices [1]). To be more specific, NDVI has been widely recognized for its crucial role in assessing vegetation coverage [2], [3], [4], guiding ecological protection [5], [6], and informing urban planning and agriculture [7], [8]. In addition, many studies highlight the pivotal role of NDVI in application for crucial ecosystems, such as forest management and grassland conservation, by offering essential data support for ecological protection initiatives [9], [10], [11]. Moreover, the use of NDVI enables the monitoring of the intricate relationships between vegetation and outside disturbance. Notably, it is a helpful tool to study the interaction between vegetation and climate factors [12], [13], [14], [15]. This is particularly valuable during natural disasters, as it facilitates the assessment of the impact of events, such as floods, droughts, and frostbite [16], [17], [18], [19]. Considering its versatility, as reasoned above, researchers have devoted considerable efforts toward acquiring high-resolution NDVI data for Earth surface monitoring.

The acquisition of long time-series and high-resolution NDVI datasets remains a significant challenge for many scholars due to the inherent tradeoff between spatial and temporal resolutions. Although enhancing spatial resolution yields more details, it often comes at the expense of reduced temporal resolution, thereby restricting data availability and limiting the full realization of the data's potential use. Further challenges are the coarse temporal resolution and the presence of mixed pixels within NDVI data, both of which impede the product's application in surface cover change detection and classification. In particular, the 0.05° advanced very-high-resolution radiometer (AVHRR) NDVI dataset, despite its extensive time series, underperforms in capturing detailed texture information. To reconcile the balance between time and spatial resolution, a plethora of research is redirecting their focus toward the NDVI downscaling techniques.

Manuscript received 25 November 2023; revised 25 February 2024; accepted 3 March 2024. Date of publication 6 March 2024; date of current version 29 March 2024. This work was supported by the National Natural Science Foundation of China under Grant 42090012. *(Corresponding author: Xiang Zhao.)*

Mengmeng Sun, Xiang Zhao, Siqing Zhao, Yinkun Guo, Wenxi Shi, and Longping Si are with the State Key Laboratory of Remote Sensing, Science, Beijing Normal University, Beijing 100875, China, also with the Institute of Remote Sensing and Digital Earth, Chinese Academy of Sciences, Beijing 100875, China, and also with the Beijing Engineering Research Center for Global Land Remote Sensing Products, Faculty of Geographical Science, Institute of Remote Sensing Science and Engineering, Beijing Normal University, Beijing 100875, China (e-mail: smm2021@mail.bnu.edu.cn; zhaoxiang@bnu.edu.cn; zhaosi-qing@mail.bnu.edu.cn; guoyinkun_bnu@mail.bnu.edu.cn; wenxi_shi@mail.bnu.edu.cn; silongp@bnu.edu.cn).

Jiacheng Zhao is with the Key Laboratory of Ecosystem Carbon Source and Sink, China Meteorological Administration (ECSS-CMA), Nanjing University of Information Science and Technology, Nanjing 210044, China (e-mail: jzhao@nuist.edu.cn).

Naijing Liu is with the POWERCHINA Northwest Engineering Corporation Limited, Xi'an 710065, China (e-mail: liunj@mail.bnu.edu.cn).

Digital Object Identifier 10.1109/JSTARS.2024.3373884

Conventional downscaling techniques include interpolation methods, reconstruction-based methods, and machine-learning methods. The interpolation-based techniques predominantly employ a designated pixel as the central point and calculate the values of its neighboring pixels through diverse interpolation methodologies. These methods have computational efficiency but also indistinct boundaries [20], [21]. To improve the indistinct boundaries, many reconstruction-based methods have been proposed, which aim to improve the precision and level of detail in the resulting downscaling image by utilizing prior knowledge [20], [22]. Nevertheless, these methods cannot capture high-frequency information [23]. To address this, many researchers have turned to machine-learning methods. These methods rely on extensive training data to establish a direct relationship between low-resolution and high-resolution images. However, their effectiveness can be limited and it may lead to the loss of high-frequency information [24], [25], [26], mainly when dealing with the nonlinear mapping relationship between low-resolution images and high-resolution images. This highlights the need for further advancements in downscaling methods to address these complex nonlinear correlations.

The exploration and extraction of nonlinear attributes have seen significant progress, with researchers developing a variety of feature combinations. A landmark development in this area is the downscaling convolutional neural network (CNN), which employs bicubic interpolation alongside a three-layer convolutional network to create high-resolution images, demonstrating the robust capabilities of deep learning in the realm of image downscaling reconstruction [27], [28]. This method, however, extracts only a limited set of features by relying on information from a singular image. To bypass this shortcoming, Tong et al. applied the DenseNet network architecture combined with a 1×1 convolutional kernel and a skip structure, enabling the transfer of low-level image features to higher levels. This strategy facilitated the extraction of a broader range of image features, yielding significant results, albeit with certain limitations in the context of multiperiod images [29], [30]. To better efficiently realize the feature transfer, Lim et al. [23] introduced the multiscale downscaling architecture that allowed parameter sharing among multiple architectures, expediting convergence and reducing parameter count. Furthermore, Wang et al. proposed the residual network (ResNet), a method that integrates deep and shallow strategies in network design and utilizes an external network to efficiently transfer gradients, thereby enhancing learning effectiveness and overall model performance. This approach emphasizes the potential of varying network depths in optimizing downscaling methods [23], [32].

As the complexity of the network increases, degradation in model training becomes a more significant issue. Researchers proposed ResNets that add skip connections to regular layers, providing shortcuts by adding a layer's input to its output. For example, He et al. [33] proposed ResNets to simplify the deep networks. Sdraka et al. [34] introduced two main strategies, including global residual learning (GRL) and local residual learning (LRL). GRL aims to learn the residual between input and output images, recovering high-frequency details. Concurrently, LRL represents the insertion of local shortcuts between intermediate layers to alleviate the vanishing gradient problem at the network depth [35]. Residual learning is widely used in image super-resolution networks, including the residual dense network [36], very deep super resolution [37], and enhanced deep super resolution [23]. ResNets cannot sufficiently deal with intricate and varied feature types. The development of multiscale network topologies is aimed at enhancing feature learning intensity. Multiscale networks, by employing characteristics of various sizes, aim to improve the network's expressiveness and flexibility. Subsequent investigations delved into the reconstruction of multidimensional features.

To increase multivariate coupling in the downscaling process, it is a common practice to impose additional meteorological variables as inputs [38], [39]. In downscaling processes, the choice of auxiliary data is usually related to the physical meaning and relevance of the target variables. For example, for precipitation downscaling, DeepSD [40] and Nest-UNet [41] utilize static terrain feature elevations as an auxiliary predictor for generating more accurate patterns in complex terrains. Several studies have explored the interaction between vegetation growth and topography by incorporating topography-related auxiliary data, such as digital elevation models (DEMs). Considering China's diverse vegetation, complex terrain, and significant climate changes, the adaptability of the vegetation index downscaling model encounters major challenges. Therefore, developing a super-resolution vegetation index for areas with complex vegetation and topography is crucial. Despite the demonstrated effectiveness of deep-learning methods in addressing nonlinear relationships and restoring high-resolution images, the sheer volume of data generated presents notable challenges in terms of computer storage performance. The current research focus leans toward enhancing various aspects of the neural network model, including architecture, activation function, and optimization methods [24], [25], [42], [43]. Through comparative analyses, improvement of visual representation activation function [43], [44], [45] and optimization methods [46], [47] can improve the computational efficiency and provide more accurate mappings than traditional techniques [31], [48].

Despite the numerous studies on downscaling algorithms and the relentless efforts of many researchers, the aforementioned issues have been partially resolved. However, the following challenges still need to be overcome and improved: 1) utilizing multiscale data flows to generate a high-resolution vegetation product is particularly challenging in forest areas with complex terrain and high spatial heterogeneity; and 2) the statistical relationships applied in the downscaling process may vary between different regions and lack stability, which are especially evident in complex terrain areas like forests [49].

A sophisticated downscaling technique is introduced to address the issue previously discussed. This novel approach has been thoroughly validated and competes strongly with Landsat 5 (1982–2000) and moderate resolution imaging spectroradiometer (MODIS) NDVI (2001–2015) data in the studied areas. The empirical results confirm the effectiveness of the multiscale residual CNN (MRCNN) method for use in both complex and flat terrains. The results demonstrate the suitability of the MRCNN technique for application in regions characterized by

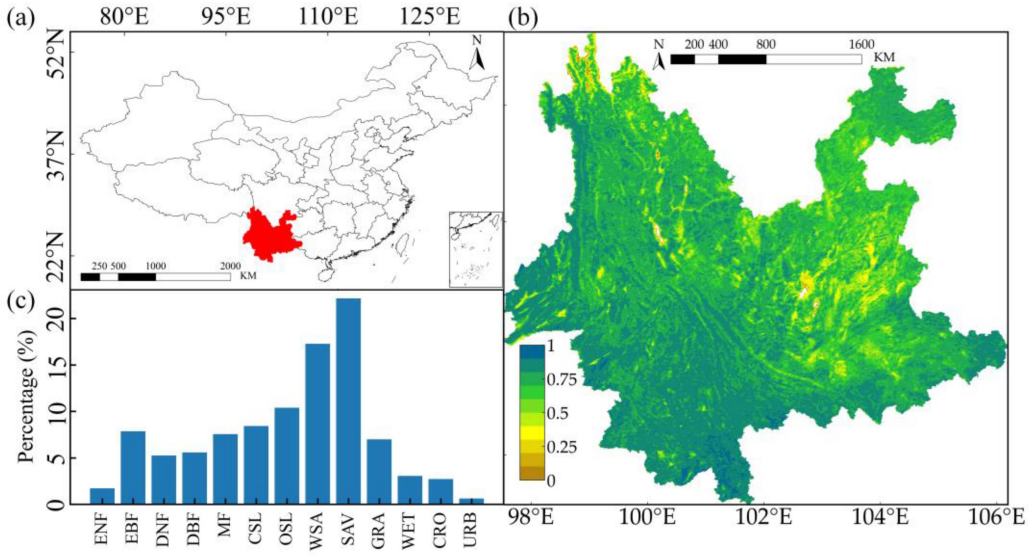

Fig. 1. Overview of the study area. (a) Yunnan Province location map in China. (b) Distribution of various categories. (c) MOD13A2 spatial map for July 28, 2015, in Yunnan Province, China. Note: ENF: evergreen needleleaf forest; EBF: evergreen broadleaf forest; DBF: deciduous broadleaf forest; MF: mixed forest; CSL: closed shrubland; OSL: open shrubland; WSA: woody savanna; SAV: savanna; GRA: grassland; WET: permanent wetland; CRO: cropland; and URB: urban.

intricate topography as well as in regions with level terrain. This article addresses pertinent challenges prevalent in contemporary research, notably: 1) the daunting task of leveraging multiscale data streams to produce vegetation productivity at high resolutions, particularly in densely wooded regions marked by intricate topography, diverse environmental conditions, and pronounced spatial heterogeneity; and 2) the instability and variability of statistical correlations employed in the downscaling process across different regions, particularly in rugged terrains like forests. The main contributions of this article are as follows.

1) This article generates an efficient technique to address challenges in downscaling AVHRR NDVI in areas with complex geography and diverse vegetation.

2) Creating a simulated MODIS NDVI data dataset at 1-km spatial resolution, covering 1982 to 2015. The new dataset can investigate how changes in regional ecological contexts impact vegetation indicators and evaluate their potential to yield important insights.

The rest of this article is organized as follows. Section II outlines the study area and data datasets utilized in the article. Section III provides an in-depth account of the implemented algorithm and methodology. Section IV presents the model results and offers a comparison with analogous products, including quantitative and qualitative analyses. Sections V hosts an extensive discussion. Finally, Section VI concludes this article.

II. Study Area and Datasets

A. Study Area

The distinct geographical location of Yunan contributes to its diverse climate types. The region features a warmer and more humid environment. The areas enjoy an all-year spring climate favorable for cultivating various crops. The northwest typically experiences arid and semiarid climates characterized by abundant sunshine, extended precipitation periods, and substantial evaporation. The southeastern region, with its frequent precipitation, four distinct seasons, and semihumid to humid climate, experiences monsoons (Fig. 1). Furthermore, the diverse topography of Yunnan, ranging from coastal plains to inland mountains and plateaus at elevations of thousands of meters, contributes to its extraordinarily complex climatic zoning. Its climate is divided into eight subregions based on variations in precipitation and altitude. Distinct climate features of each subregion contribute to a varied and unique climate system. This diversity creates favorable conditions for preserving biodiversity and agricultural output yet poses challenges for researchers. Adapting the vegetation index downscaling model becomes more challenging due to the numerous vegetation types, complex terrain, and significant climate fluctuations.

Situated on the southeastern edge of the Qinghai–Tibetan Plateau within China's Yunnan–Guizhou Plateau, Yunnan province presents a varied topography marked by towering mountains, rolling hills, expansive basins, and plains, lying betwixt 21°8'32"–29°15'8" N latitudes and 97°31'39"–106°11'47" E longitudes [Fig. 1(a)].

This geological heterogeneity precipitates a wide spectrum of elevations, with a peak differential of 6663.6 m, fostering a unique mosaic of climates and ecosystems. The vegetational diversity encompasses a range spanning tropical rainforests, warm temperate coniferous forests, evergreen broadleaf forests (EBFs), evergreen needle-leaf forests, and deciduous broadleaf forests [Fig. 1(b)]. This array, constituting 62.4% of the total forest cover, is integral to maintaining ecological equilibrium and elucidating the evolutionary trajectories of distinctive vegetation types. Given these biomes' representativeness and the broad spectrum of vegetation types, this article employs EBFs, evergreen needleleaf forests (ENF), mixed forests (MF), woody savanna (WSA), and savannas (SAV) as test subjects to assess the performance of the MRCNN method for downscaling NDVI.

A spatial distribution map based on MOD13A2 data reveals a predominant NDVI value range of 0.4–0.8 for Yunnan Province, indicative of relatively high vegetation coverage, particularly in areas represented in deep blue [Fig. 1(c)]. This high vegetation coverage underscores the province's importance in fostering ecosystem health and biodiversity.

B. Datasets

Xiao et al. generated 8-day 0.05° AVHRR NDVI data from 1982 to 2015 as low-resolution input. It consists of daily gridded NDVI products with a spatial resolution of 0.05°, equivalent to approximately 5550 m [50], [51]. Due to its early establishment, real-time significance, and extensive spatial coverage, this article has chosen the AVHRR image data as a valuable source for long time-series data.

The MOD13A2 dataset, which possesses a spatial resolution of 1 km and a temporal resolution of 16 days, serves as a crucial remote sensing resource for examining vegetation growth and alterations on a global scale [52]. The creation of the MOD13A2 dataset signifies a collaborative effort between the United States Geological Survey (USGS) and NASA, leveraging the MODIS sensor on the Terra satellite. In this article, the data processing approach encompasses utilizing the MRT tool and Python programming language to execute a series of operations, including batch splicing, projection transformation, and cropping, on the MOD13A2 dataset. The outcome of this intricate procedure yields tailored MOD13A2 data that specifically caters to the ecological and geographical characteristics of Yunnan Province, spanning a timeframe of 15 years from 2000 to 2015.

The Shuttle Radar Topography Mission Digital Elevation Model 30 m (SRTM DEM 30 m) signifies a groundbreaking effort to generate extensive worldwide digital elevation information. This dataset is meticulously crafted through radar instruments on the space shuttle, facilitating precise and distinct measurements of the Earth's surface. As a result, the SRTM DEM 30 m creates a comprehensive digital elevation dataset that covers the entire Earth, demonstrating an impressive spatial resolution of approximately 30 m per pixel. The acquisition of accurate topographic data is of utmost importance due to its significant implications in various disciplines, including geographical information systems, geomorphology, and remote sensing. It is crucial to acknowledge that this endeavor necessitates essential preprocessing methodologies, such as resampling and cropping, to ensure the optimal performance and applicability of the DEM. It can be obtained from CGIAR—CSI via the hyperlink: http://srtm.csi.cgiar.org (January 13, 2024, retrieved).

Yang and Huang [53] produced the annual China Land Cover Dataset (CLCD) based on 335 709 Landsat images on Google Earth Engine, which contains annual land cover information for China from 1985 to 2019. The CLCD is now a publicly accessible 30-m resolution long-term annual land cover dataset. It is compared with current land cover thematic products and demonstrates strong alignment with global forest change, global surface water, and impervious surface time-series datasets. Simultaneously, it illustrates the swift urbanization trend and various ecological initiatives in China, unveiling human-induced influences on LC amid climate change scenarios and offering potential value for global change research applications.

Between March 1984 and November 2011, Landsat 5 TM collected observation data in the reflected wavelength with a resolution of 30 m. The global Landsat data are stored at the Earth Resources Observation and Science Center of the USGS, where archived Landsat 5 TM data show different coverage areas [54], [55]. For better consistency among relatively clear Landsat scenes, spectral radiance can be converted to planetary or exoatmospheric reflectance by normalizing for solar irradiance [56], [57], [58]. In the formula for calculating NDVI, NIR stands for near-infrared band, corresponding to band 4 of Landsat 5; Red refers to the red band, corresponding to band 3 of Landsat 5.

III. Methodology

The MRCNN methodology enables more comprehensive training and efficient prioritization of relevant image regions. The multiscale group, residual group, upsampling module, and residual block are critical components of the MRCNN (Fig. 2). A unique network structure is created by integrating and superimposing elements and channels with the help of the ResNet and a multiscale network. The multiscale group consists of several multiscale blocks, which are used to learn the flexible multiscale features to enhance the diversity of extracted features. In addition, the numerous residual blocks and convolutional networks are used to improve the learning abilities of the entire network. This groundbreaking network design holds significant potential for enhancing the effectiveness of various applications (Fig. 2).

The structure of MRCNN: This article adopts a multiscale network structure incorporating convolution blocks of sizes 3×3, 5×5, and 7×7, designed to learn multiscale features beneficial for highlighting boundary details. Furthermore, adopting a ResNet architecture, as opposed to a dense fusion strategy, strengthens interlayer learning and reduces the number of parameters and computational load, thereby improving processing efficiency. In addition, PixelShuffle operates by breaking down the input low-resolution image into basic pixel blocks. These blocks are rearranged according to learned mapping relationships, synthesizing a high-resolution image. This method surpasses traditional interpolation techniques in both reconstruction quality and computational efficiency. What is more, a specialized module for terrain and land cover feature extraction is designed, targeting high-resolution terrain data to extract multiresolution features. Finally, we introduced residual block design to blend high-frequency and low-frequency data to further improve the quality of the predicted images achieving a more balanced internal detail and clearer edges.

The introduction of high-resolution terrain feature extraction and multiscale feature extraction modules is crucial as they capture more details and information during analysis, essential for enhancing model precision and reliability. By combining features extracted from high-resolution terrain data, CLCD, and AVHRR NDVI data, the method applies an integrated approach to various scales and depth features, improving the model's capability to capture terrain details and analytical accuracy. This

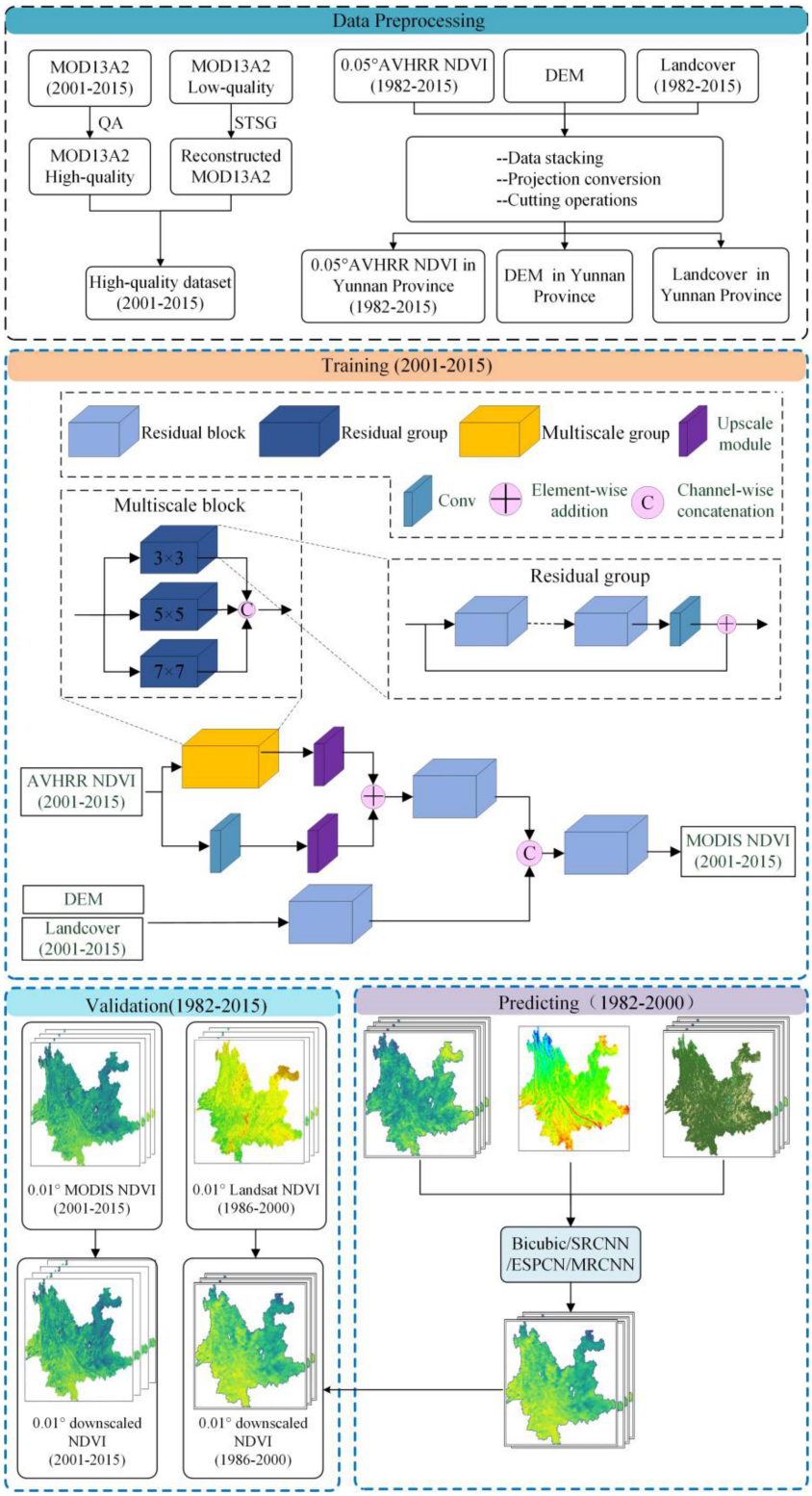

Fig. 2. Flowchart of the image downscaling process. Abbreviations: SRCNN—super-resolution convolutional neural network. ESPCN—efficient subpixel convolutional layer. MRCNN—multiscale residual convolutional neural network.

method, by merging multiple data sources and techniques, enhances the quality and efficiency of feature extraction, providing rich and precise data support for subsequent analysis. It considers multiple factors, such as terrain and vegetation, resulting in more comprehensive and reliable analytical outcomes. To further improve model precision, specialized modules for terrain data and land cover feature extraction, along with multiresolution feature fusion, are specifically designed. To demonstrate the effectiveness of high-resolution terrain data extraction and multiscale feature fusion modules, these modules are introduced

into the MRCNN model. Results indicate that including auxiliary data significantly reduces the disparity between MODIS NDVI and Landsat 5, confirming the modules' contribution to revealing finer details.

The neural network architecture comprises four essential components: the residual group, the multiscale group, the upsampling module, and the residual block (Fig. 2).

The input layer: The postpreprocessed AVHRR data (1982–2015) served as input with the DEM data for training the method.

The residual group, depicted as a dark blue rectangle, consists of interconnected residual blocks. Each residual block contains two convolutional layers and an element summing operation, facilitating the capture of high-frequency image details.

The multiscale group, represented by an orange rectangle, consists of multiple parallel residual groups. The features processed by each residual group are combined with the features obtained from convolutional network processing. This combination is achieved by performing an elementwise summation operation and aids in the recovery of low-frequency image details. Different sizes of convolutional kernels (3×3, 5×5, and 7×7) are used to extract features from various sensory field angles, and channel-level concatenation enhances the network's performance.

The upsampling module: The model is illustrated as purple rectangles, and it enlarges the image size by a factor of five using the PixelShuffle technique. PixelShuffle accomplishes this by converting low-resolution feature maps into high-resolution feature maps through convolution and channel reorganization. This method effectively enlarges the image, replacing traditional interpolation or deconvolution techniques.

Conv: It is depicted as a sky-blue rectangle, representing the convolution operation.

The output layer is used to complete the downscaling of the NDVI data and generate the 1-km resolution NDVI dataset for the years 1982 to 2015. The output layer employs different loss functions and evaluation metrics to optimize the network parameters.

For AVHRR NDVI data, two branches are deployed for processing. The first branch employs a multiscale group to extract diversified features, which are subsequently fed into the upsampling module to generate a 1-km resolution feature map. The second branch utilizes convolution operations to derive new features, which are then input into the upsampling module to create a 1-km resolution feature combination. The feature maps produced by the two branches are integrated using elementwise addition to formulate a new feature map, denoted as Feature Map 1. For the input DEM data, features are extracted via residual blocks to form Feature Map 2. Feature Map 1 and Feature Map 2 are then channel level connected to create Feature Map 3. This map undergoes further processing via residual blocks to ultimately yield the 1-km resolution MODIS NDVI data.

The specific steps are as follows:

Data preparation: The 0.05° AVHRR NDVI data (1982–2015) underwent several data processing steps, such as batch splicing, projection transformation, cropping, bidirectional reflectance distribution function (BRDF) adjustment [41], [42], [43] and other procedures to generate the Yunnan Province AVHRR NDVI data. High-resolution target data came from 16-day 1-km resolution MODIS NDVI datasets covering 2001–2015. Quality pixels from MOD13A2's quality assurance filtering were retained. Spatial–temporal Savitzky–Golay (STSG) processing [59] was used to reconstruct low-quality pixels affected by clouds, snow, and aerosols. High-quality region pixels were preserved, while low-quality ones were replaced with reconstructed values using STSG. Each image size is 850×797, totaling 345 images. The MODIS NDVI images were split into 75% training and 25% validation sets. DEM and CLCD served as auxiliary data alongside AVHRR NDVI as the input datasets. DEM data provided terrain height information aiding in downscaling, while land cover data improved accuracy and textural detail. During model training, MODIS NDVI served as output data.

Features extraction: Model performance was assessed by analyzing loss function values of both training and validation datasets, with the model exhibiting the lowest loss being deemed optimal. The optimal model was trained on 0.05° AVHRR NDVI data to simulate 1-km MODIS NDVI images. Model effectiveness and accuracy were evaluated by comparing high-resolution NDVI images produced by the model with actual MODIS NDVI images. The model selection was based on the criteria being the smallest root mean squared error (RMSE) value and mean absolute error (MAE) value. After comparing these parameters and undergoing parameter adjustment and optimization, we selected the optimal model to complete the downscaled task and got them ready for performance comparison. We used the MRCNN network to generate a new dataset and compared it with the 1-km high-quality MODIS NDVI. If the new dataset demonstrates the best agreement with the high-quality MODIS NDVI data, the model can estimate the NDVI dataset before 2000. In addition, we use Landsat 5 to validate the new dataset spanning from 1982 to 2000. The study employed 1-km MODIS NDVI data from 2001 to 2015 as the validation dataset, enabling the analysis and assessment of the 1-km NDVI data within the same temporal scope. We used the spatial distribution of RMSE and MAE to check the single pixel of the new NDVI dataset from 1982 to 2015.

The findings from the 15-year testing of the downscaling data indicated a robust concordance between our approach and the impact of MODIS NDVI data. In addition, our method exhibited durability when subjected to prolonged sequence testing. Furthermore, we selected five biomes to confirm their robustness and applicability. The results showed that the proposed MRCNN method can effectively capture more complex texture information and enhance the learning performance of the algorithm. These meticulous operations have improved the accuracy and facilitated the acquisition of long-term NDVI data. This substantial contribution enables the investigation of vegetation growth before 2000 and the analysis of environmental changes.

IV. Results

A. Comparison of Downscaled NDVI Products Obtained by the MRCNN Method With Other Methods

1) Accuracy Evaluation of Various Downscaled Methods: After applying downscaling techniques, such as bicubic, SRCNN, ESPCN, and MRCNN, to AVHRR NDVI data and

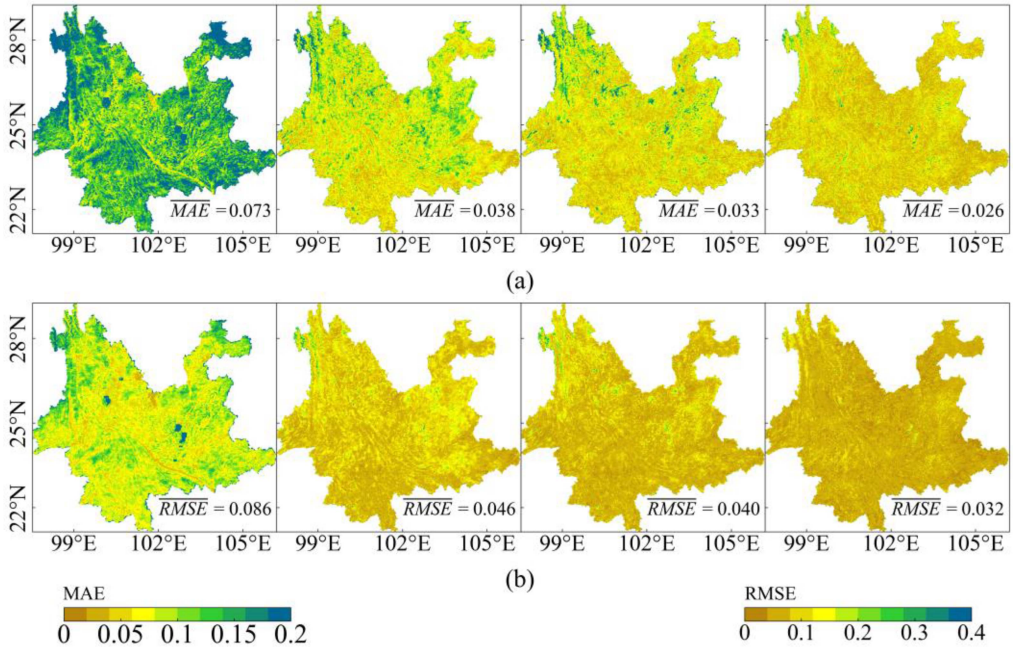

Fig. 3. Spatial distribution of MAE and RMSE across various methods in 2015. (a) MAE spatial distribution. (b) RMSE spatial distribution. Left to right: bicubic, SRCNN, ESPCN, and MRCNN.

comparing the results with MODIS NDVI data, we found 1) the mean MAE values were 0.073, 0.038, 0.033, and 0.026, respectively, [Fig. 3(a)]; and 2) the mean RMSE values were 0.086, 0.046, 0.040, and 0.032, respectively, [Fig. 3(b)]. Qualitative analysis of spatial distribution maps for MAE and RMSE indicates that the MRCNN algorithm significantly enhances texture information compared to AVHRR NDVI. The MRCNN algorithm reduced MAE and RMSE by 0.026 and 0.032, respectively, with a 64.38% improvement for MAE and a 62.79% improvement for RMSE compared to AVHRR NDVI. This evidence underscores the MRCNN algorithm's downscaling efficacy in complex and plain terrains. The marked reductions in MAE and RMSE emphasize the superior performance of the MRCNN algorithm and broad applicability across diverse landscapes and vegetation types. This evidence confirms the MRCNN algorithm as a crucial tool for enhancing NDVI data resolution and accuracy, vital for ecological monitoring and analysis. It can be mainly attributed to the MRCNN, which focuses on the differences between AVHRR NDVI and MODIS NDVI in specific regions, thus increasing the importance of these mapping features.

To examine the long-term stability of the MRCNN method's performance, we comprehensively compared different downscaled products using a long-term analysis across five distinct vegetation biomes in Yunnan province. It involved detailed scrutiny of the annual mean NDVI curves for these biomes (ENF, EBF, MF, WSA, and SAV) from 1982 to 2015. The objective was to evaluate how effectively four notable downscaling techniques captured interannual trends and seasonal cycles (Fig. 4). Results highlighted that the MRCNN method's downscaling results mirrored the reference data most closely across all biome classes. The result suggests the MRCNN method's superior capability in effectively recreating different vegetation biomes. Conversely, the ESPCN and SRCNN techniques underestimated the NDVI value, especially during the summer. The results could be due to their shortcomings in handling intricate feature classes during the downscaling procedure. This finding aligns with the variations observed in the time-series curves in 2015 (Fig. 4). Moreover, there was a significant discrepancy between the bicubic downscaling results and the reference data. The results can be traced back to the bicubic method's inability to capture high-frequency specifics, resulting in inadequate downscaling tasks. These findings proved the stability of the MRCNN method, the time, and the feasibility of applying the MRCNN method proposed in this article to solve the long time-series studies in different biomes. To comprehensively validate the practical effectiveness of our downscaling algorithm, we also tested the time series of NDVI. As shown in Fig. 5, the outcomes generated by our MRCNN method downscaling algorithm exhibited the closest alignment with MODIS NDVI for the five representative biomes. These findings emphasize the effectiveness and superiority of our technique in accurately describing the vegetation dynamics in all five biomes from 1982 to 2015 concerning its advantage of spatiotemporal consistency. The commonly used two metrics to compare different deep-learning methods are peak signal-to-noise ratio (PSNR) and structural similarity index (SSIM) [60], with the former testing the ratio of the resulted pixels to the noise pixels and the latter describing the statistical similarity of the MODIS NDVI reference image and the different downscaling results. The results of this article indicate that SSIM and PSNR fluctuate with seasonal changes. This finding underscores the impact of environmental factors on these critical image quality metrics. After comparing various super-resolution techniques, including MRCNN, SRCNN,

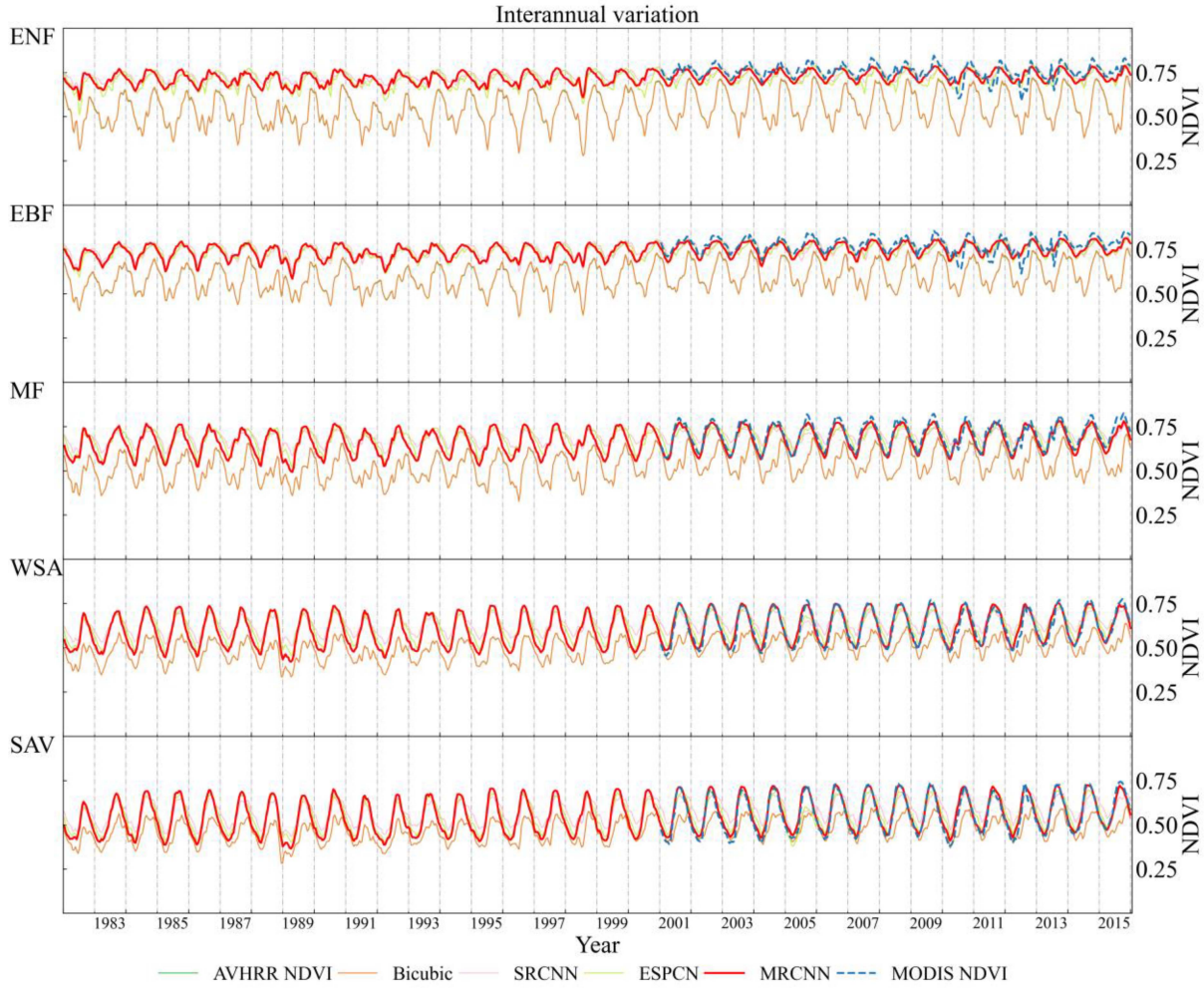

Fig. 4. Time-series curves of typical species obtained by different methods, spanning 1982 to 2015.

ESPCN, and bicubic, the MRCNN method demonstrated superior performance. Specifically, compared to bicubic, the MRCNN method showed a 28.5% improvement in PSNR and a 16.2% improvement in SSIM, corresponding to numerical increases of approximately 4 and 0.12, respectively, (Fig. 6). The findings show that MRCNN consistently outperformed alternative methods, including SRCNN, ESPCN, and bicubic method.

B. Spatial Distributions Evaluation of Downscaled NDVI Products Obtained by Various Downscaled Methods

NDVI spatial distribution maps are crucial tools in environmental and ecological fields, enabling the monitoring of vegetation health and growth over time. They offer insights into environmental changes, aid in agricultural management, reveal biodiversity distribution, highlight urbanization impacts, and support postdisaster assessment. These maps are instrumental in research and making decisions across various domains.

Fig. 7 serves as a visual representation of the effectiveness of four distinct downscaling techniques, illustrated through the spatial distribution maps of the resulting 1-km NDVI downscaling products. The maps are arranged in sequential order from left to right, commencing with the 1-km NDVI data and followed by the results garnered from SRCNN, ESPCN, and ultimately, the MRCNN method. This arrangement allows for a precise comparative analysis of each technique's effectiveness. Upon close inspection, it becomes apparent that the MRCNN method's downscaling outputs are similar to the 1-km NDVI data, underscoring its advanced ability to capture intricate texture details. In contrast, while the SRCNN and ESPCN methods demonstrate some capability in capturing texture information, their results do not align as closely with the 1-km NDVI data as the MRCNN method.

Moreover, the bicubic method exhibits noticeable shortcomings, with certain regions lacking texture information, emphasizing its relative inadequacy in contrast to the other techniques. Fig. 7(a) presents a spatial distribution that displays detailed textures. These results suggest that 0.05° AVHRR NDVI exists in several overestimated or underestimated areas, which is inconsistent with the 1-km MODIS NDVI. Compared to MRCNN, there are fewer instances of overestimation or underestimation, especially in areas characterized by complex terrains or diverse

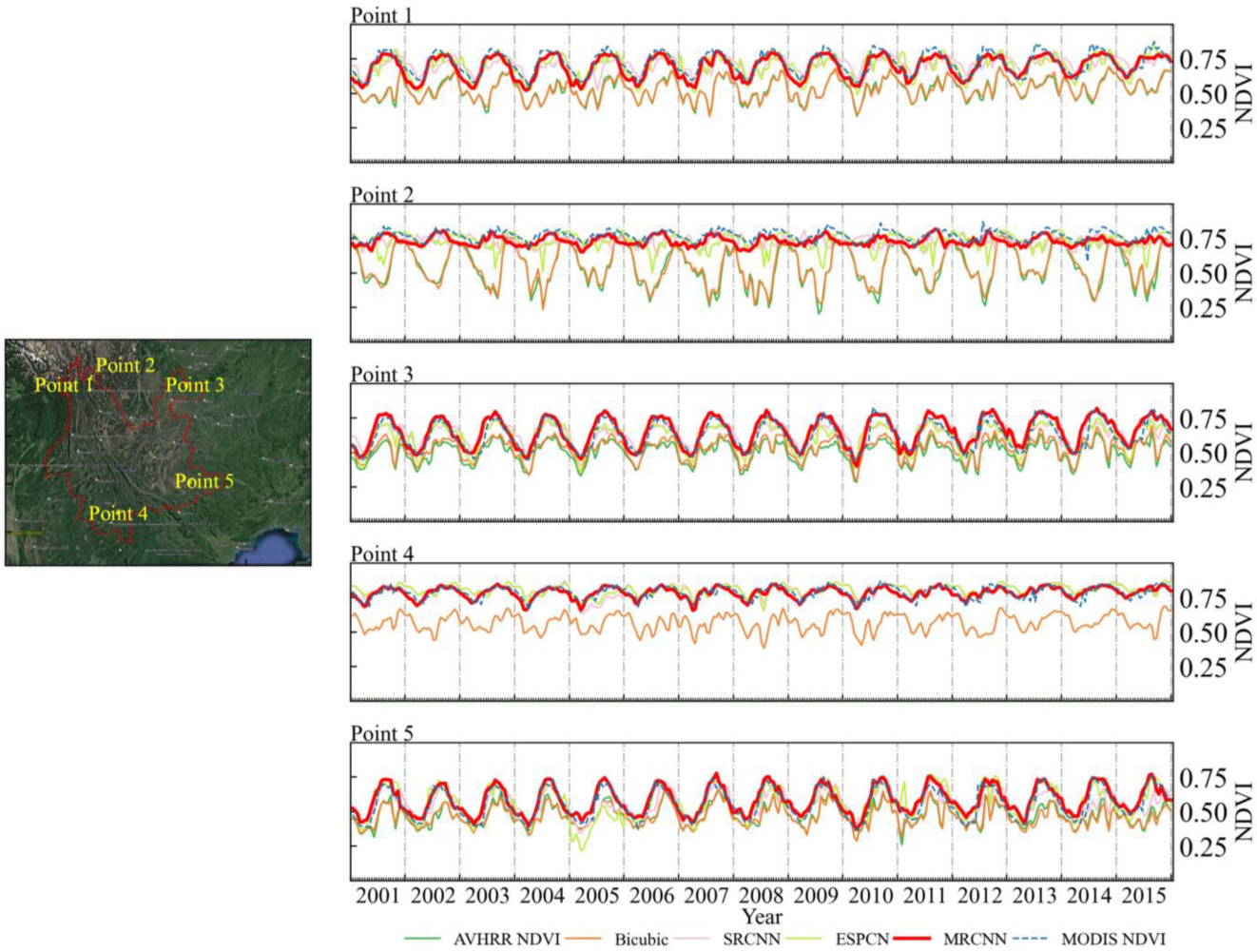

Fig. 5. Downscaled results at five random points with five typical biomes using different methods. Note that: Point 1. MF; Point 2. ENF; Point 3. WSA; Point 4. EBF; Point 5. SAV.

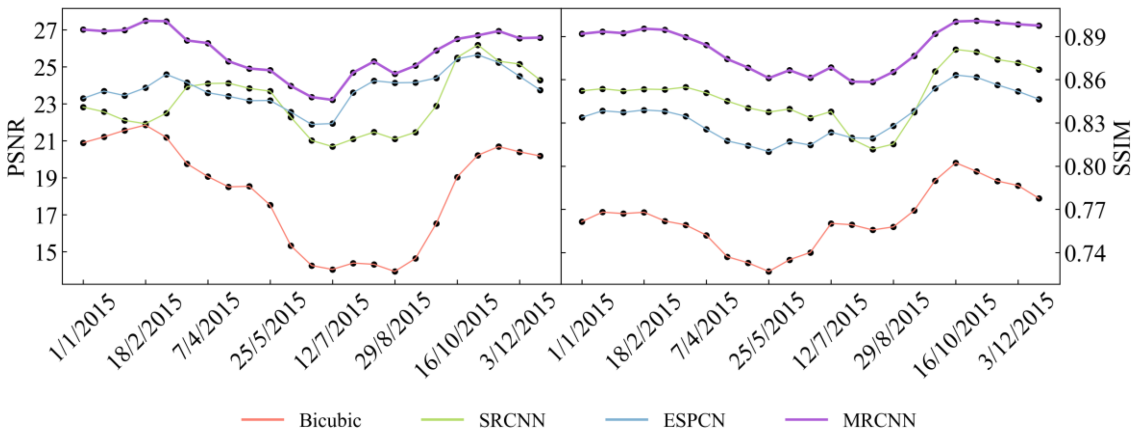

Fig. 6. Time-series curves of PSNR and SSIM with various methods in 2015.

vegetation. This indicates that the effectiveness of these methods subtly differs depending on the geographical characteristics of the regions. The density distribution graph depicts inflection points at 0.4 and 0.6. Within the 0.4–0.6 interval, the bicubic technique slightly overestimates, while between 0.6 and 0.8, it markedly overestimates. SRCNN exhibits underestimations in the 0.2–0.6 intervals, and overestimations occur from 0.6 to 0.8 (Fig. 7(b)). ESPCN also presents minor underestimations in the 0.2–0.5 ranges, with modest overestimations noted in the 0.6–0.8. Despite occasional underestimation or overestimation,

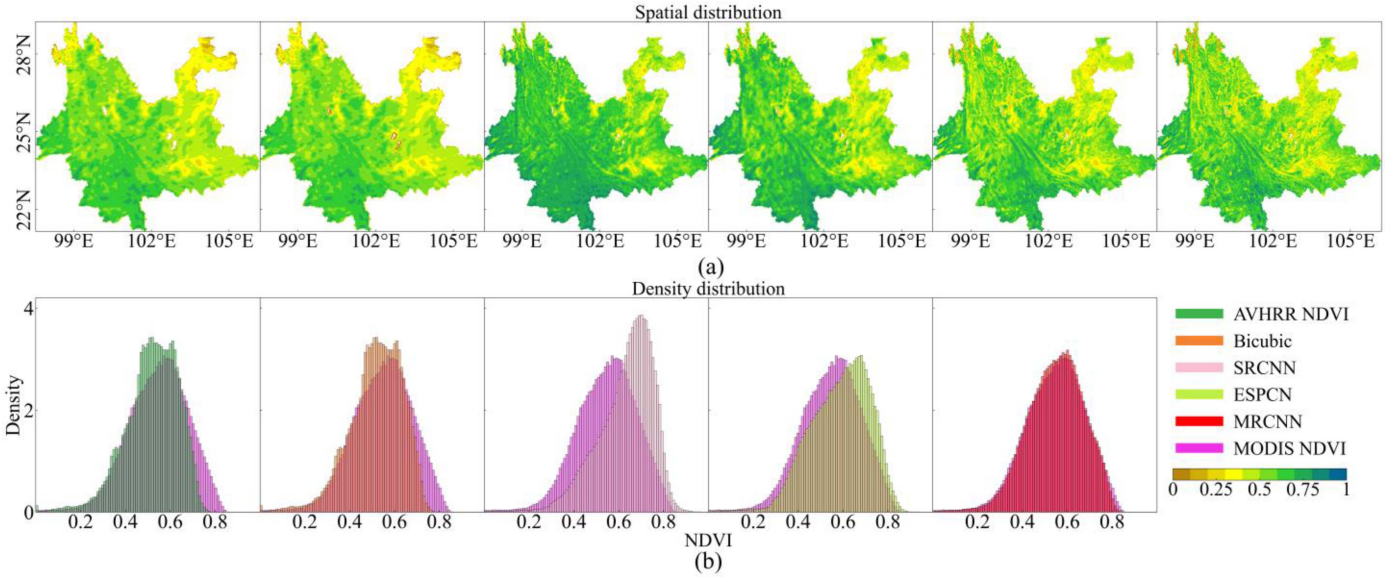

Fig. 7. Results of various downscaled methods in 2015. (a) Spatial distribution of NDVI mean values by various downscaling methods. (b) Density distribution of NDVI mean values by various downscaling methods. Note: AVHRR NDVI, bicubic, SRCNN, ESPCN, the MRCNN, and MODIS NDVI.

MRCNN downscaling outcomes align closely with MODIS NDVI, showcasing unparalleled precision and alignment with actual vegetation indices.

An accurate assessment of the vegetation index is crucial for comprehensively understanding vegetation dynamics changes, particularly in areas characterized by complex topography. Consequently, selecting appropriate downscaling techniques is imperative for precisely capturing change information and addressing changes across different temporal scales. The findings illustrate the spatial distribution data of NDVI obtained through various downscaling methods across multiple temporal scales, such as daily and monthly (Figs. 8 and 9).

Fig. 8 plays a significant role in assessing the consistency of NDVI value variations with MODIS NDVI for selected months in 2015. More specifically, the figure represents each quarter of 2015 with January, April, July, and October. The image analysis shows seasonal variations in the NDVI, indicating a consistent underestimation of NDVI values by AVHRR NDVI compared to MODIS NDVI across all seasons. The MRCNN algorithm greatly enhances NDVI. This improvement is consistently observed throughout winter, spring, summer, and autumn, with significant enhancements during the spring, summer, and autumn seasons. Compared to MODIS NDVI, the areas improved by the MRCNN algorithm exhibit a higher level of consistency. These findings demonstrate that the MRCNN algorithm significantly improves AVHRR NDVI, enhancing its utility for monitoring seasonal vegetation changes. It highlights the ability of four downscaling methods to reflect seasonal growth patterns of vegetation, showcasing their performance across different times of the year. The bicubic approach, however, struggles with accuracy in complex terrains, leading to significant underestimations or overestimations. While SRCNN and ESPCN also encounter difficulties accurately capturing vegetation in such terrains, MRCNN distinguishes itself by significantly reducing these errors and closely aligning with MODIS NDVI data, proving the most effective in accurately mapping vegetation across varied landscapes. Spatial distribution maps of NDVI values for these chosen months are juxtaposed with corresponding MODIS NDVI values, which allows for a direct and clear comparison. Upon careful analysis of these maps, it becomes evident that the MRCNN method is highly effective in incorporating texture, and its results align closely with those of the MODIS NDVI.

Conversely, the ESPCN and SRCNN methods present sporadic instances of underestimation in specific regions and a comparatively limited ability to capture texture. Most notably, the bicubic method displays substantial underestimation and a poor ability to capture textures. Thus, this figure underscores the MRCNN method's superior ability to match the consistency of MODIS NDVI values. In addition, MRCNN excels in accurately identifying regions characterized by complex vegetation types and aligns more closely with MODIS NDVI in areas with subtle border distinctions (Fig. 8).

To test the algorithm's robustness, we chose areas of the downscaled results of Yunnan's complex terrain and rich species area as the small window zoom. Fig. 9 illustrates the outcomes of image scale reduction using various methods for a specific day in July 2015. These methods include MRCNN, ESPCN, SRCNN, and the bicubic method. By comparing their results, one can observe the distinct effectiveness of each technique in capturing and representing the spatial arrangement of NDVI values. For instance, the MRCNN method demonstrates its efficacy by accurately capturing and conveying the spatial distribution of NDVI values for this particular day.

In contrast, the ESPCN and SRCNN methods occasionally underestimate the values, as dashed squares indicate. In addition, the downscaling result by SRCNN provides more spatial details than ESPCN. The bicubic method, however, suffers from considerable underestimation and exhibits a limited ability to capture

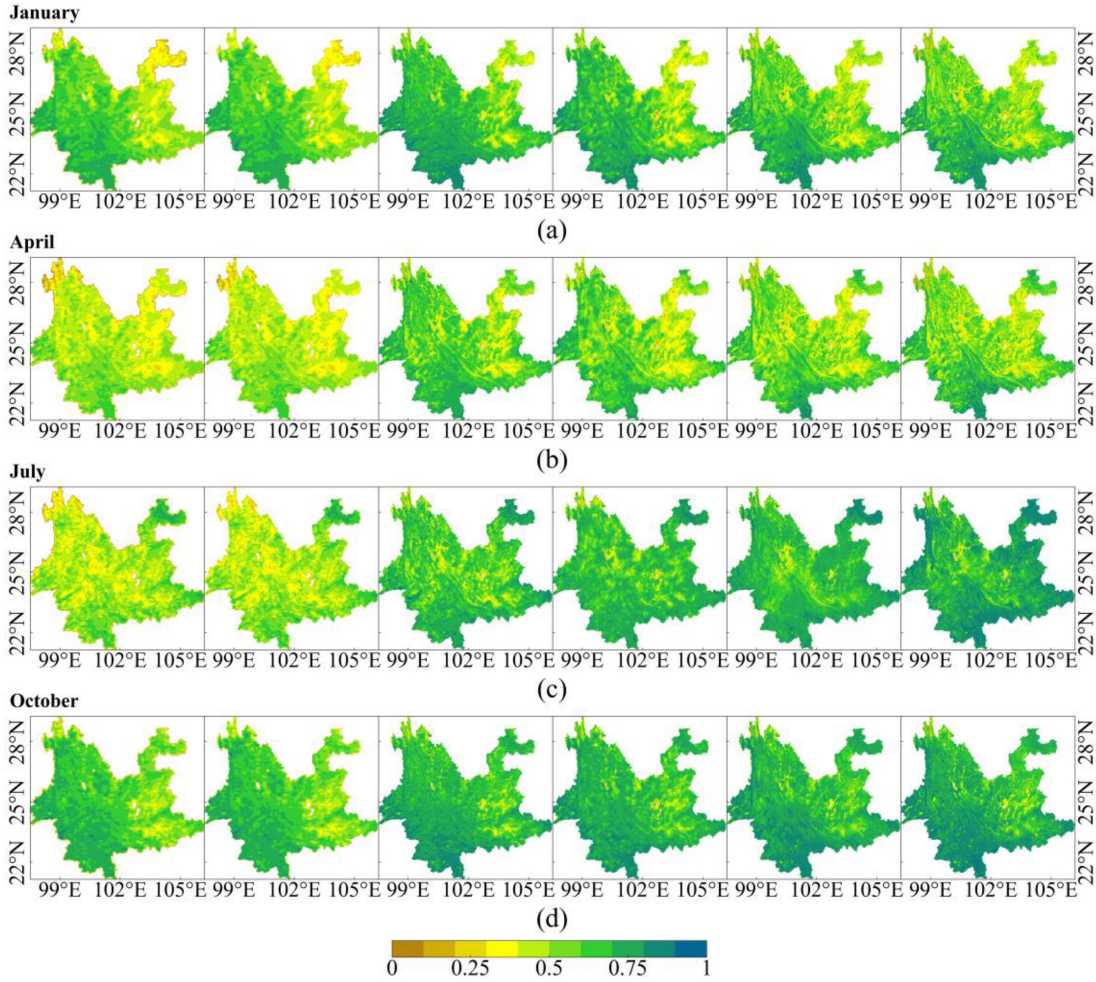

Fig. 8. Spatial distribution of NDVI through different downscaling techniques in 2015. January, April, July, and October correspond to the winter, spring, summer, and autumn, respectively. (a) January; (b) April; (c) July; and (d) October. From left to right: AVHRR NDVI, bicubic, SRCNN, ESPCN, MRCNN, and MODIS NDVI.

textures effectively. This comparison underscores the superior performance of the MRCNN method in achieving precise image scale reduction. The results show that compared with MODIS NDVI, AVHRR NDVI lacks a lot of most of the texture information. The downscaled effect of the MRCNN algorithm increases a lot of texture information compared with AVHRR NDVI, and the added information is highly consistent with MODIS NDVI.

C. Validation of the Downscaled Produces (1982–2015)

1) Validation of the Algorithm With High-Quality MODIS NDVI Data (2001–2015): To evaluate individual performance and quantify the tangible effects of downscaling methods, we employed scatter plots to visually present the results obtained from the 2015 dataset (Fig. 10). The article specifically assessed downscaling phenomena by measuring RMSE and MAE, which are important indicators of the accuracy and effectiveness of the downscaling techniques used. The results indicate that the MRCNN technique achieved the lowest values for these parameters (Fig. 10). Furthermore, compared with AVHRR NDVI, the MRCNN downscaled results were highly concentrated along the 1:1 line, exhibiting MAE of 0.032, RMSE of 0.045, and R^2 of 0.874 [Fig. 4(b)]. Regarding error reduction, the study noted a decrease in RMSE by 0.112 and a reduction rate of 71.3%. Similarly, the accuracy of MAE improved by 0.102 and a reduction rate of 25%. In addition, the R^2 metric showed an improvement of 0.12 and an improvement rate of 76.1% (Fig. 10). This suggests that it offers greater accuracy and performance than other techniques, such as ESPCN and SRCNN. On the other hand, the bicubic interpolation process yielded the least desirable outcomes. Furthermore, the scatter plot revealed a high concentration level in our method, as evidenced by the close alignment of the distribution with the 1:1 line.

These findings provide empirical evidence supporting the effectiveness of our downscaling methods and highlighting their ability to achieve remarkable consistency with validation data. In addition, these results underscore the potential of our technique to improve the usability of MODIS NDVI data.

2) Validation of the Algorithm With Landsat Data (1982–2000): Given the high susceptibility of Landsat data to cloud cover, obtaining cloud-free images that comprehensively cover Yunnan Province proves challenging. Therefore, a section of

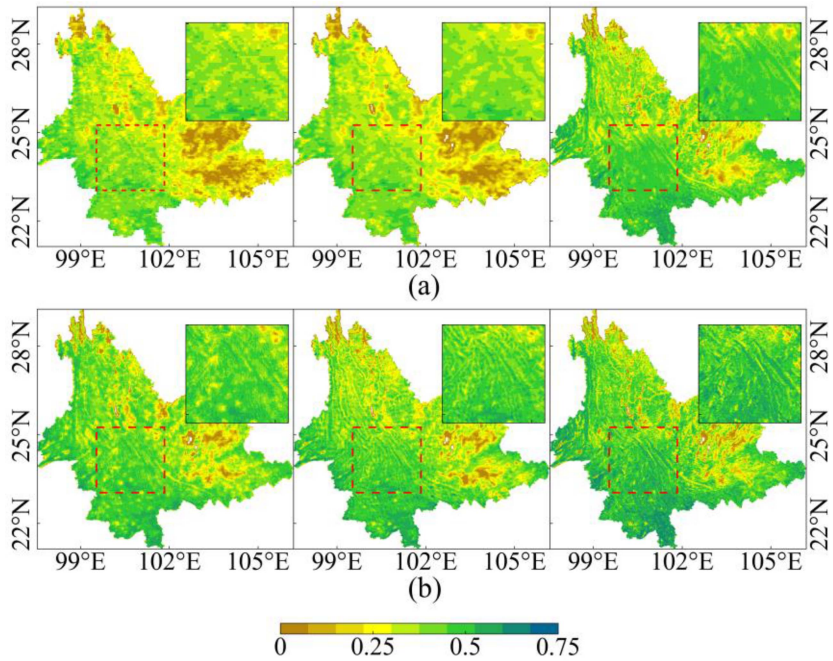

Fig. 9. Spatial distribution of Yunnan province on 24 July 2015, zoom in to display local texture detail information. Note: left to right (a) AVHRR NDVI, bicubic, SRCNN; and (b) ESPCN; MRCNN, and MODIS NDVI.MRCNN.

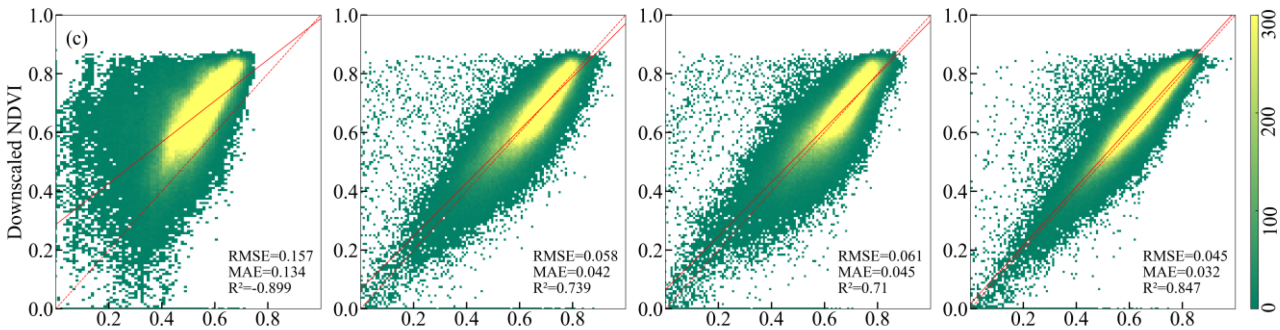

Fig. 10. Density scatterplots for different downscaled methods in 2015 throughout Yunnan province. Dashed lines represent 1:1 lines, while solid lines indicate the best-fit lines derived from linear regression. From left to right: bicubic; SRCNN; ESPCN; and MRCNN.

Yunnan Province with less than 5% cloud cover was selected for validation analysis. Moreover, discrepancies in the validation results are inevitable due to spectral range and spectral response function differences among various data sources. Typically, the higher the similarity between the original and target data, the more effective the downscaling process. However, a comparison between AVHRR NDVI data and Landsat data reveals significant differences, contributing to substantial discrepancies in the outcomes. Before validating with Landsat 5, its data need to be upscaled to 1 km. Then, Landsat 5 data from 1982 to 2000 is used to validate the simulated data obtained for the same period.

Typically, the higher the similarity between the original and target data, the more influential the downscaling process. However, a comparison between AVHRR NDVI data and Landsat data reveals significant differences, contributing to substantial discrepancies in the outcomes. Before validating with Landsat 5, its data need to be upscaled to 1 km. Then, Landsat 5 data from 1982 to 2000 is used to validate the simulated data obtained for the same period.

There is a significant correlation and similarity between MODIS NDVI and AVHRR NDVI, making the use of MODIS NDVI to validate the downscaled data results from 2001 to 2015 relatively reliable and accurate. The NOAA–AVHRR satellite series has a 20-year global NDVI data record, and combining MODIS–NDVI data will provide a more extensive and longer data series for practical monitoring and research. The MODIS vegetation index uses a new synthesis algorithm to reduce biases caused by changes in observation angles and the solar target sensor geometric relationship. In generating vegetation index grid data, molecular scattering, ozone absorption, and aerosol correction algorithms will be used, and the BRDF model will be utilized to correct observation data.

Some problems lie about the spatiotemporality consistency. Several factors contribute to uncertainties in AVHRR-based

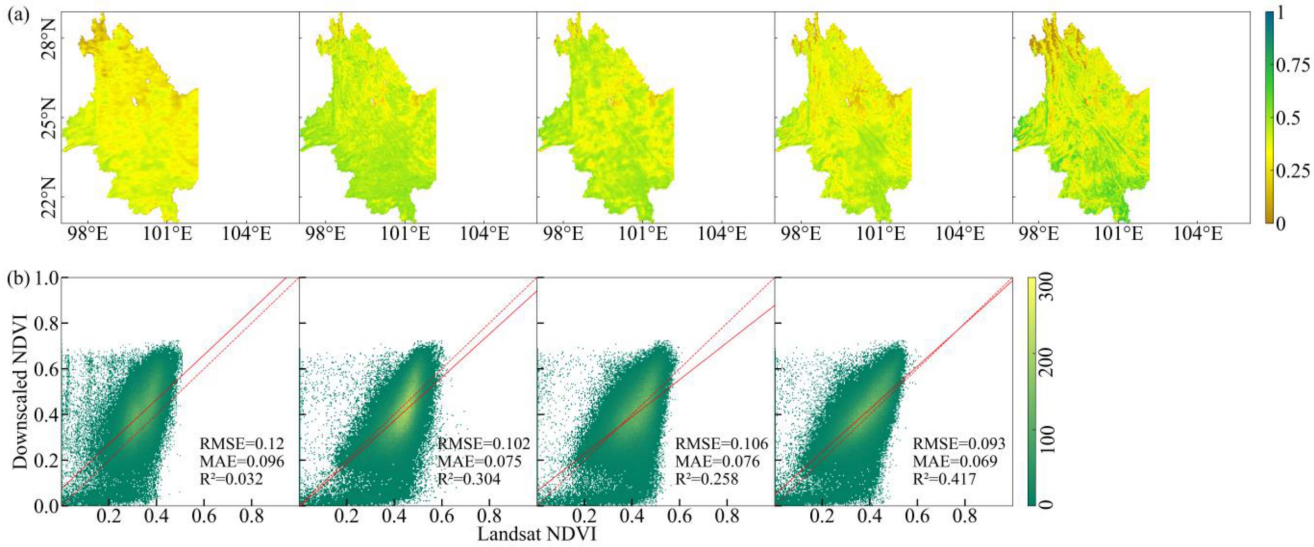

Fig. 11. Density scatterplots for different downscaled methods in February 1994 throughout Yunnan province. Dashed lines represent 1:1 lines, while solid lines indicate the best-fit lines derived from linear regression. From left to right: AVHRR NDVI; bicubic; SRCNN; ESPCN; and MRCNN.

NDVI products. Initially, variations in band configurations, such as center wavelength and spectral response function, among AVHRR sensors (like AVHRR-2 and AVHRR-3) and between these and other sensors (for example, MODIS and VIIRS), play a significant role [61], [62], [63], [64]. Second, NDVI discrepancies among identical AVHRR sensors on different NOAA satellites may also arise. Here, variations in image capture times and sun-target-sensor geometries between sensors can lead to a "jump" (a sudden shift in values) in the NDVI time series [65], [66], [67], [68]. For instance, the AVHRR sensor aboard NOAA-11 exhibits a significantly higher NDVI compared to the AVHRR sensors that came before and after it [69]. Third, the accuracy might be compromised by the orbital drift of NOAA satellites and the deterioration of AVHRR sensors, which is attributable to the severe conditions in outer space [70]. Artificial signals within the orbital drift in moist regions were noticeable for AVHRR-derived NDVI products (e.g., VIP3 NDVI, LTDR4 NDVI, and GIMMS NDVI3g) and subsequent products like the GIMMS leaf area index [71].

This discrepancy results in MAE and RMSE values when directly evaluating the reconstruction outcomes using Landsat data (Fig. 11). An initial attempt to align Landsat data with MODIS through linear fitting (though its effectiveness is uncertain) precedes the evaluation of metrics. Furthermore, the results indicate that MRCNN is feasible for estimating data before 2000. The inherent value differences between Landsat and MODIS NDVI datasets significantly impact the MAE and RMSE calculations, which rely heavily on the discrepancies between the reconstructed and reference images.

V. Discussion

A. Adaptability of Mixed Pixel Phenological Characteristics

The box plots provide a detailed analysis of the statistical properties of NDVI data for five specific biomes (EBF, ENF, MF, WSA, and SAV) during different seasons. At the same time, the growth status of five typical vegetation types during the growing season is also displayed in box plots (Fig. 12). Each plot represents the distribution of NDVI data for a particular biome, including vital statistical measures, such as the maximum, minimum, median, and upper and lower quartiles. These plots serve as a valuable tool for understanding the effectiveness of different downscaling methods across various biomes and seasons. The box plots show that the MRCNN method exhibits a strong correlation with the MODIS NDVI for WSA and SAV during spring, further strengthening in autumn.

In addition, the density plots provide insight into the distribution of NDVI values and their consistency with the MODIS NDVI. These plots enhance our understanding of the impact of downscaling on NDVI value distribution. The density plots clearly show that the results of the MRCNN method closely align with the peak values of MODIS NDVI, while the bicubic method displays the most significant deviation. In conclusion, the informative charts effectively compare and evaluate the performance of different downscaling methods in processing NDVI data (Fig. 12). These findings offer valuable guidance for future article and applications.

Boxplots provide a detailed analysis of the statistical features of NDVI data for five different biomes across different seasons and throughout the entire growth period (Fig. 12). These charts are a valuable tool for understanding the effectiveness of other downscaling techniques across various biomes and seasons. The density distribution map reflects the proportion of NDVI mean values in different ranges.

Fig. 12 illustrates the NDVI mean value trends across various vegetation types (EBF, ENF, MF, WSA, and SVA) throughout the four growing seasons, highlighting distinct growth patterns for each type, as follows.

1) EBF growth trend analysis: The NDVI mean values for EBF are consistently around 0.78 throughout the year, indicating minimal seasonal variation. The NDVI obtained by the MRCNN

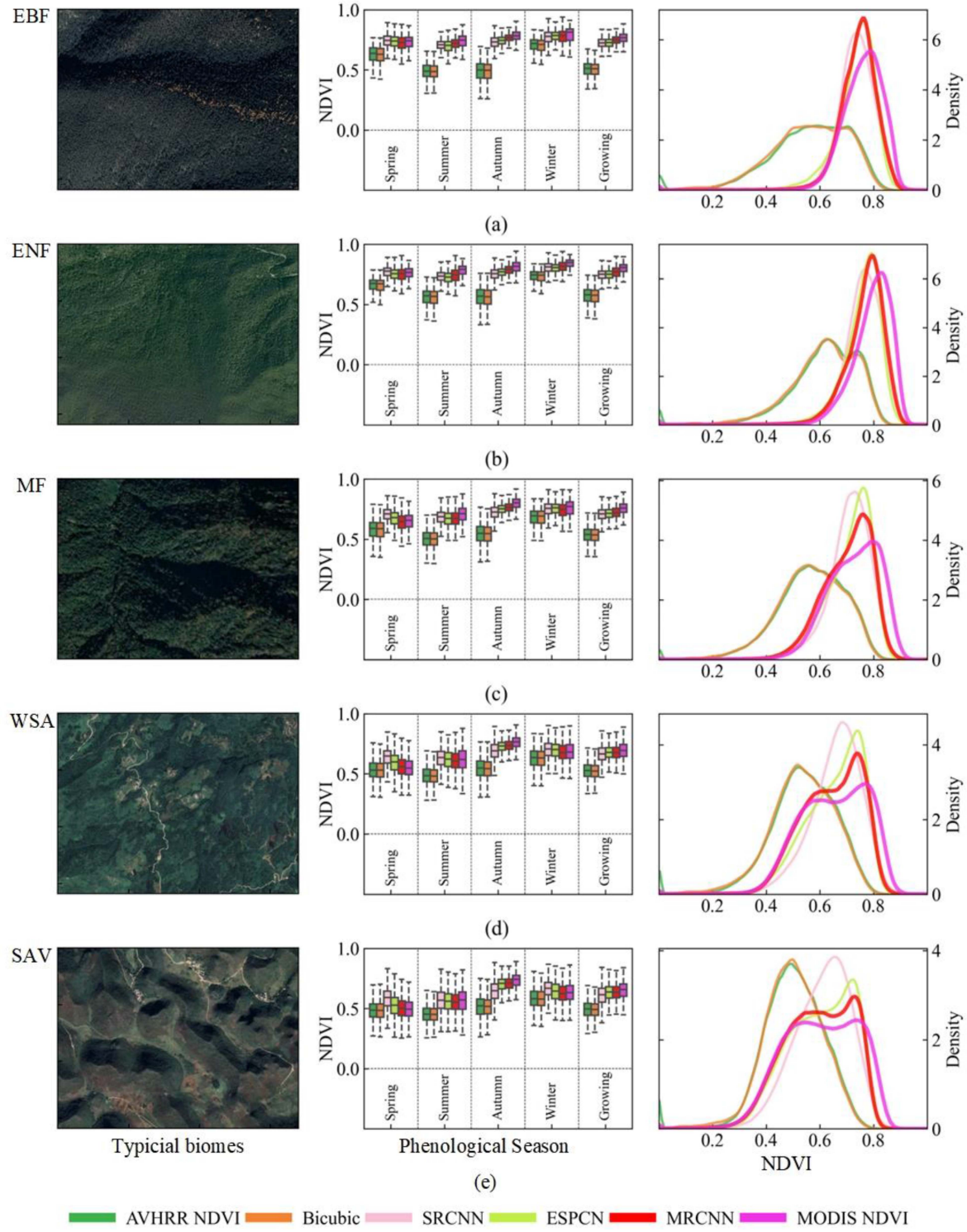

Fig. 12. Downscaled results of various biome categories using different methods in 2015 in Yunnan province. Left to right: images of typical ecosystems selected from Google Earth; boxplots showing downscaled results for different methods including spring, autumn, summer, winter, and the growth season; and density distribution of downscaled results for different methods: (a) EBF; (b) ENF; (c) MF; (d) WSA; and (e) SAV.

method aligns closely with the MODIS NDVI mean, showcasing superior accuracy and improvement over the AVHRR NDVI, which averages around 0.5. The density distribution further reveals that MRCNN 's NDVI means are predominantly around 0.78, mirroring the MODIS NDVI distribution, albeit with a slight tendency toward overestimation. This contrasts starkly with AVHRR's NDVI, which is concentrated around 0.58, underscoring its substantial underestimation.

2) ENF seasonal growth pattern: ENF's NDVI mean values also exhibit slight annual fluctuation, stabilizing around 0.80. Again, the MRCNN method demonstrates the closest approximation to MODIS NDVI's mean value. The density

distribution maps corroborate the MRCNN 's enhanced performance and slight underestimation compared to MODIS NDVI, which has its most significant proportion of mean values around 0.8. AVHRR NDVI's largest proportion, around 0.60, reflects a significant underestimation, underscoring MRCNN 's substantial accuracy improvement.

3) MF growth dynamics: MF shows an apparent seasonal variation in NDVI mean values, with winter and autumn around 0.42, spring around 0.75, and summer peaking at 0.75. The MRCNN NDVI mean is closest to MODIS NDVI, significantly improving upon AVHRR NDVI's average of 0.55. MRCNN and MODIS NDVI's most significant proportions of mean values cluster around 0.72, indicating high consistency and MRCNN's notable advancement over AVHRR NDVI.

4) WSA seasonal trends: WSA's NDVI means display seasonal trends, with MRCNN reflecting the closest correlation to MODIS NDVI's growth trend. The density distribution shows MRCNN and MODIS NDVI's most significant proportion of means around 0.78, attesting to their consistency. MRCNN 's substantial improvement over AVHRR NDVI is evident, with AVHRR's largest proportion of means at 0.55, highlighting significant underestimation.

5) SVA seasonal growth analysis: SVA exhibits distinct seasonal NDVI mean values, with MRCNN closely mirroring MODIS NDVI's trend, particularly noticeable in the peaks around 0.45 and 0.76. AVHRR NDVI, primarily concentrated around 0.50, starkly underestimates the mean NDVI values compared to MODIS NDVI, emphasizing MRCNN 's substantial enhancement in capturing the accurate growth status of ENF.

Overall, Fig. 12 underscores MRCNN's superior performance in closely matching MODIS NDVI's mean values across different vegetation types and seasons, highlighting its effectiveness in accurately capturing the growth trends and improving upon the limitations observed in AVHRR NDVI outputs. In spring, the MRCNN method demonstrates a robust association with MODIS NDVI for the MF, SAV, and WSA ecological communities. Concurrently, the correlation between the two biomes further intensified during autumn. At the same time, bicubic exhibits the most notable difference. A line graph and the boxplot display the correlation between downscaled results and MODIS NDVI. In addition, the results indicate that NDVI demonstrates a seasonal variation. For example, the warming and moistening of the North Atlantic warm current and the cooling and drying effects of the winter cold current collectively contribute to the seasonal changes. The results show that the AVHRR NDVI is consistently underestimated for the selected biological groups, persisting throughout the year. The results of MRCNN indicate overestimation for ENF, EBF, MF, and DBF in winter, but they align well with MODIS NDVI in other seasons. SRCNN and ESPCN models show unstable underestimation or overestimation, indicating that these approaches have complex nonlinear variations in their applicability across different biological communities and experience seasonal fluctuations.

NDVI temporal curves and growth trend lines offer invaluable insights for scientists, agricultural experts, and environmental managers in environmental monitoring, resource management, and climate change research. It is reasonable to utilize NDVI temporal curves and growth trend lines presenting the downscaled results. It becomes evident that the proposed MRCNN method approach outperforms all the other methods in terms of achieving a closer alignment with the mean phenology curves of 1-km NDVI data and capturing the annual trend of NDVI (Fig. 13). The results of temporal curves, growth trend lines, and the spatial distribution analysis of the mean NDVI trend indicate that the MRCNN method produces the closest approximation of the mean values characterizing the growth change trend (Fig. 13). In contrast, the 1-km NDVI downscaled results from all the other methods all showed the underestimation of mean NDVI annual trend found in southwestern Yunnan province compared to the reference data from MODIS NDVI. These regions embody high vegetation dynamics because of the elevation heterogeneity, and only the proposed MRCNN method tackles this problem efficiently (Fig. 13).

In presenting downscaled results, the MRCNN method has demonstrated a superior ability to align with the growth patterns observed in MODIS NDVI. Specifically, this method closely approximates the mean value characterizing growth change trends, displaying a high level of congruity throughout all the months. Compared to other methods, the MRCNN approach outperforms aligning with the mean phenology curves of 1-km NDVI data and capturing the intra-annual NDVI trend (Fig. 13).

Besides, the algorithm MRCNN demonstrates superior performance in capturing single-year results and maintaining consistency with the MODIS NDVI trend. As can be seen from the annual time-series chart, the downscaled 1-km NDVI shows the highest concordant level (23.50E-4) with the trend value of MODIS NDVI (35.59E-4) (Fig. 13). Beyond mere trend value comparison, the MRCNN algorithm also excels in capturing the single-year results and maintaining consistency with the MODIS NDVI trend (Fig. 13). The annual time-series chart shows the MRCNN method's downscaled 1-km NDVI aligning most closely with the trend value of MODIS NDVI. However, all other techniques exhibit varying degrees of uncertainty, overestimating the NDVI trend at different levels.

Moreover, the MRCNN method performs remarkably well in aligning with the 1-km MODIS NDVI's interannual trend, effectively capturing the evolving trends' characteristics. This is apparent in the discernible downward trends in 2002, 2008, and 2011, and varying degrees of upward trends in 2003, 2009, and 2012 (Fig. 13). However, it is important to note that other methods, such as the bicubic approach, ESPCN method, and SRCNN, show some inconsistency with the observed MODIS NDVI change patterns (Fig. 13).

The reliability of the MRCNN method is particularly highlighted in its ability to estimate data before 2000. This feature enhances its referential value and makes it a robust tool for long-term ecological and environmental studies. Furthermore, the MRCNN method's precise estimation of changes in vegetation growth states and trends is instrumental in various applications. It aids in identifying growth cycles, understanding how vegetation responds to seasonal climate variations, detecting shifts in land use, and assessing the impacts of climate

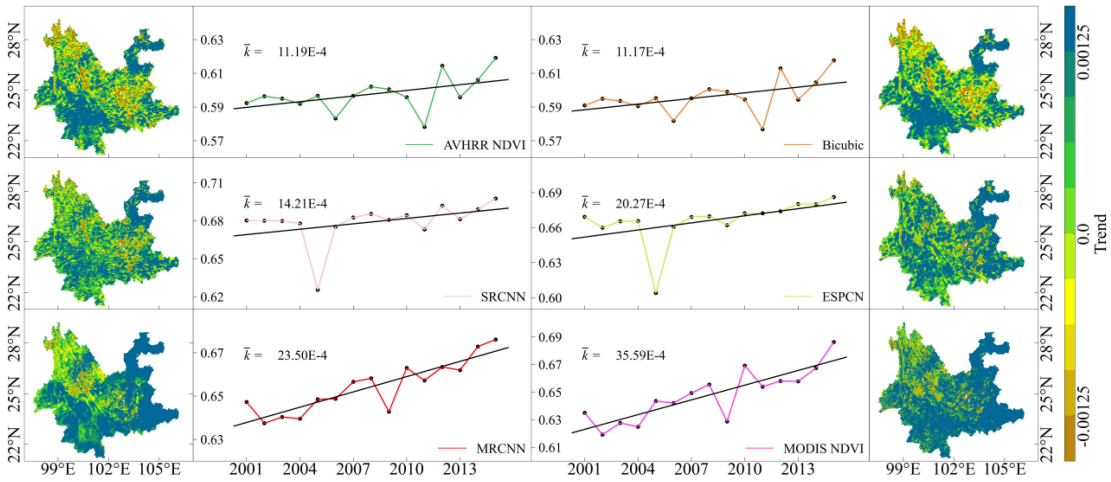

Fig. 13. Growth trend lines and spatial distribution analysis of mean NDVI trends in Yunnan. Row 1: AVHRR NDVI, bicubic interpolation; Row 2: SRCNN, ESPCN interpolation; Row 3: MRCNN method, and MODIS NDVI data.

change. Faced with natural disasters, the NDVI data generated by the MRCNN method plays a pivotal role in evaluations, providing critical insights into changes in vegetation. These data are also essential in agricultural management, helping guide irrigation, fertilization, and harvesting decisions. In biodiversity conservation, the precise NDVI data can assist in identifying ecologically sensitive areas and biodiversity hotspots. Thus, it provides a scientific basis for planning and managing these areas. In conclusion, the accuracy and reliability of the MRCNN method make it a valuable tool for scientists, agricultural specialists, and environmental managers who rely on such data for research and making decisions.

Prior research has explored how spatial resolution affects leaf phenology tracking in temperate areas through observations from multiscale remote sensing. For instance, Zhang et al. [72] discovered that using imagery with a coarse spatial resolution introduced uncertainties in land surface phenology, as evidenced by a comparison with phenology derived from fine-resolution imagery. Chen et al. [73] carried out a simulation study and discovered that significant uncertainty in phenology extraction is linked to coarser spatial resolution and the mixing of plant species, a discovery further validated by Liu et al. [74] and Tian et al. [75] utilized real-world satellite data. Similar effects of mixing can be expected in tropical forests as the spatial resolution varies, owing to the combination of various forest components (namely, bare branches, leaves, and shade in our context) within each pixel. This aggregation impacts both the spectral and spatial characteristics of the pixels [76], [77], leading to ambiguities in characterizing tropical phenology. Nonetheless, the influence of spatial resolution on measuring tropical leaf phenology, as estimated through the deciduousness metric, is still insufficiently investigated.

These investigations also revealed that a coarser spatial resolution might increase uncertainty in monitoring phenology [74], [78]. The fundamental mechanism is complex, yet it can primarily be attributed to the growing mix of species with the expansion of pixel size, which diminishes the likelihood of pure pixels in images of coarser resolution [79], [80]. This is especially pertinent in tropical landscapes filled with evergreen trees, where the crowns of deciduous trees make up a minor portion of the canopy and are thinly scattered across the terrain [81], [82].

B. Comparison With Previous Studies

The article introduces MRCNN, a novel image downscaling approach, which merges residual and multidimensional networks, designed to preserve original image data, particularly high-frequency details, for high-quality results. The MRCNN method demonstrated a higher correlation with the 1-km MODIS NDVI values, surpassing other algorithms and closely mirroring the 1-km MODIS NDVI in the ENF, EBF, and MF categories [83], [84], [85]. This finding underscores the reliability, robustness, and accuracy of our proposed approach, consistently generating the most favorable outcomes across all seasons and growth periods [86], [87], [88].

To comprehensively assess and validate our downscaling algorithm's efficacy in practical applications, we carefully selected five distinct feature types, encompassing a range of both natural and artificial surface characteristics, such as typical forests, farmlands, and grasslands (Fig. 4). We randomly selected a point from each feature and followed their time-series curves from 2001 to 2015 (Fig. 5). This methodology allowed for extensive and long-term observations, leading to a thorough understanding of the practical implications and significance of downscaling.

Building on this foundation, this article focused on a specific timeframe, treated as an autonomous, discrete interval. This approach facilitated a detailed examination of the alignment between the downscaling outcomes and the MODIS NDVI, a commonly used vegetation index critical for evaluating surface attributes and monitoring changes in surface vegetation [89], [90], [91]. Comparative analysis revealed that our MRCNN algorithm produced outcomes that demonstrated a higher alignment with MODIS NDVI for the five typical features. This result indicates that our algorithm can more accurately represent the true characteristics of these features, underscoring its significant practical utility (Fig. 12). Upon conducting individual examinations of each year of the five features as separate intervals,

our method showed marginally superior alignment with MODIS NDVI compared to four other methods, reinforcing the superiority of our downscaling algorithm.

Examination of the time curves revealed that our method successfully learned richer texture information. By contrast, SRCNN and ESPCN showed a lower capacity for learning texture details, leading to some degree of underestimation. This finding underlines the enhanced accuracy of our algorithms in extracting and acquiring texture information (Fig. 6).

Through comparative analysis, we found that our MRCNN downscaling algorithm produced results that aligned significantly more with the MODIS NDVI for the selected five features. This finding suggests that our algorithm can more accurately represent the true characteristics of these features, providing substantial practical significance [92], [93], [94]. When we conducted individual examinations of each year for the five features as discrete intervals, our method demonstrated marginally superior correspondence with MODIS NDVI compared to the other four methods, despite overall improvements. This finding underscores the superiority of our downscaling algorithm. Analyzing the timing curves revealed our method's successful learning of richer texture information [Fig. 4(a)].

In contrast, it was observed that SRCNN and ESPCN exhibited a lower capacity for texture detail learning, resulting in some degree of underestimation. This highlights our algorithms' enhanced accuracy and superior texture information extraction and acquisition capability. The bilinear interpolation method showed a clear tendency to underestimate and produce fewer estimated texture details [Fig. 4(a)]. This further emphasizes our downscaling algorithm's superior accuracy and performance in dealing with diverse features compared to other methods.

When conducting individual examinations of each year of the five selected features as separate intervals, our method demonstrated marginally superior alignment with MODIS NDVI as compared to the other four methods, despite overall advancements (Fig. 6). This finding strengthens the superiority of our downscaling algorithm. Our method successfully learned to capture richer texture information by examining timing curves. Conversely, we observed that SRCNN and ESPCN demonstrated a lower capacity for learning texture details, resulting in a certain level of underestimation [95], [96], [97]. This finding underscores our algorithms' superior capability and enhanced accuracy in extracting and acquiring texture information. The bilinear interpolation method displayed a noticeable tendency to underestimate and yield fewer estimated texture details. This further highlights our downscaling algorithm's superior accuracy and performance in managing diverse features compared to alternative methods.

The dataset used in this article is important in environmental science and ecology, with implications spanning various disciplines. By utilizing the MRCNN method, we successfully transformed low-resolution NDVI data into high-resolution data. This conversion facilitates an enhanced understanding of surface vegetation cover and ecosystem dynamics. Our findings reveal detailed insights and spatial distribution patterns of NDVI data, giving us a precise knowledge of vegetation growth and overall ecosystem health. These insights are valuable for decision-makers and practitioners involved in environmental protection and sustainable development initiatives. The application of the MRCNN method has further significant implications. Specifically, transforming low-resolution NDVI data into high-resolution data allows for more effective monitoring and assessment of changes in vegetation dynamics. This is particularly crucial in agriculture, forestry, and grassland management where accurate vegetation data are vital for informed decision-making and efficient resource allocation. Furthermore, our proposed methodology advances our understanding of the complex relationship between vegetation and climate change. Through close examination and analysis of NDVI data, we can gain deep insights into how vegetation responds to climate change. This empowers us to develop improved strategies for climate change adaptation and mitigation.

MRCNN is designed to preserve original image data, especially high-frequency details, and it extracts extensive features at various scales. This approach amalgamates output and input data, maximizing the strengths of deep and shallow features. Furthermore, MRCNN employs residual blocks to tackle gradient vanishing and exploding issues and incorporates volume scaling to maintain computational efficiency while expanding the network's receptive field. As a result, MRCNN demonstrates superior downscaling accuracy and effectiveness. In addition, MRCNN utilizes a contrastive learning strategy, leveraging high-resolution images to enhance the network's adaptability to different image contents and structures. Hence, MRCNN exhibits exceptional performance in image downscaling, particularly for complex images. This superior performance can be attributed to MRCNN's unique design principles, technical resources, and learning methods, thereby outperforming other image-downscaling algorithms in accuracy, efficiency, and adaptability.

On the other hand, the conventional methods, such as SRCNN and ESPCN comparison methods used in this article, rely largely on the sample numbers. A study showcased that SRCNN has difficulty in fighting against adversarial features [98], which may explain the outcomes in Figs. 4 and 5 that SRCNN cannot adjust the NDVI value of the original AVHRR NDVI. Although the ESPCN algorithm has been proven to require less running time and feature input than SRCNN; however, the ESPCN algorithm still depends largely on the neighboring learning feature, that is, the large dependence on the surrounding pixels [99]. As a result, when it comes to the regions where the target learning feature sporadically occurs or disappears, the ESPCN yields poor performance, sometimes even worse than SRCNN [30]. As can be seen from Figs. 5 and 7, the details in southwestern Yunnan failed to be captured by ESPCN rather than SRCNN. As mentioned before, southwestern Yunnan embraces complicated elevation because of the intertwining valleys and mountains; as a result, the texture of vegetation can be very complex.

C. Limitations of the MRCNN Method

Through the analysis of five typical biomes, we can find that some challenges for the MRCNN method still exist. Regardless

of biome types, MRCNN constantly reconstructs an underestimated NDVI, which can be seen in Fig. 12. What is more, sometimes MRCNN can lead to similar performance or slightly worse than SRCNN and ESPCN, for example, in summer, winter, and growing seasons in SAV and WSA biomes. This may be due to the ignoration of seasonal changes within the training samples. In our proposed method, we have extensively changed the architecture of the neural network, but this may surrender to the requirements of very reliable samples [100]. Future article should comprehensively investigate the relationships between the MRCNN learning process and rigorous sample selection. The proposed method also requires significant computational resources and high-quality input data, which may not be readily available in some scenarios.

Furthermore, handling the long-term data series large volume and complex algorithms can pose challenges. Despite these constraints, the MRCNN represents a significant advancement in enhancing the spatial resolution of NDVI, supplementing the data gap of MODIS availability before 2000 in support of decision-making in environmental preservation and sustainable development. Continued research and improvement are necessary to optimize the method's use and contribute to environmental science and ecology advancements.

The vegetation index, a critical measure for understanding the health and status of various plant life, is influenced by an extensive array of factors that significantly complicate its analysis and interpretation. Among these factors are the ambient temperature, the amount of precipitation an area receives, and the moisture content present in the soil. This complexity is further underscored in this article, which focuses on how the vegetation index is affected by introducing additional types of data, namely DEM and detailed maps that categorize land into different classifications based on their characteristics and use. The importance of these other data types lies in their ability to provide more nuanced insights into how elevation and land use variations can impact vegetation's health and distribution across different regions. Future article endeavors are planned to expand upon this foundation by incorporating even more data sources. These efforts aim to deepen our understanding of the factors that influence the vegetation index, improving our ability to monitor, predict, and manage the natural environment more effectively.

VI. Conclusion

The present article introduces the MRCNN method, a deep-learning algorithm designed to enhance the spatial resolution of the NDVI from 5 to 1 km using historical imagery. Employing a multiscale network and a ResNet, this method facilitates extracting relevant features and the establishment of robust spatial–temporal correlation distributions between NDVI data of different resolutions. The inclusion of the DEM dataset and CLCD dataset as prior knowledge further refined the downscaling framework. Contributions of this article can be enumerated as follows: 1) the pioneering integration of the ResNet network with a multiscaled network for downscaling tasks; 2) the generation of a high-resolution 1-km NDVI dataset spanning 1982 to 2015 enhances the spatial resolution and temporal coverage of NDVI products, particularly those produced before 2000; and 3) providing detailed and accurate spatial information about vegetation changes facilitates a more comprehensive vegetation analysis. Rigorous testing confirms the compatibility of the products generated by the MRCNN method with the 1-km MODIS NDVI products.

By employing deep-learning-based downscaling techniques on 0.05°AVHRR NDVI data from 1982 to 2015, this article demonstrates the use of neural network architecture in obtaining a 1-km NDVI. The significance of this achievement lies in its ability to facilitate more accurate feature classification before 2000 and to enable the analysis of changes in the spatial and temporal attributes of these features over time. Empirical evidence supports that the downscaled data consistently capture temporal 1-km NDVI data from 1982 to 2015. This ability to acquire comprehensive and continuous datasets is crucial for analyzing pre-2000 changes in vegetation coverage. In the spatial domain, resolution has been significantly enhanced from 0.05° to 1 km, an advancement of great scientific importance. While models, such as bicubic, SRCNN, and ESPCN, have contributed to the prediction of historical MODIS NDVI, they exhibit slight underperformance across various time scales. In contrast, the MRCNN method presented in this article demonstrates superior predictive capability, accurately capturing historical MODIS NDVI data for Yunnan Province and assisting in reconstructing long-term MODIS NDVI datasets. Notably, this article marks the first application of 1-km MODIS data spanning 1982 to 2015, a breakthrough anticipated to advance research in related fields significantly.

Acknowledgment

The authors acknowledge the data support from National Earth System Science Data Center, National Science & Technology Infrastructure of China (http://www.geodata.cn), the National Aeronautics and Space Administration (NASA), the National Geospatial-Intelligence Agency, the United States Geological Survey and NASA, and Moderate-Resolution Imaging Spectroradiometer (https://modis.gsfc.nasa.gov/). The GLASS products can be downloaded at www.glass.umd.edu. The CLCD dataset introduced in this article is freely available at https://doi.org/10.5281/zenodo.4417810. DEM can be obtained from CGIAR—CSI via the hyperlink: http://srtm.csi.cgiar.org (January 13, 2024, retrieved).

References

[1] C. De Bernardis, F. Vicente-Guijalba, T. Martinez-Marin, and J. M. Lopez-Sanchez, "Contribution to real-time estimation of crop phenological states in a dynamical framework based on NDVI time series: Data fusion with SAR and temperature," *IEEE J. Sel. Topics Appl. Earth Observ. Remote Sens.*, vol. 9, no. 8, pp. 3512–3523, Aug. 2016.

[2] A. Huete et al., "Overview of the radiometric and biophysical performance of the MODIS vegetation indices," *Remote Sens. Environ.*, vol. 83, no. 1/2, pp. 195–213, 2002.

[3] Q. Meng, W. H. Cooke, and J. Rodgers, "Derivation of 16-day time-series NDVI data for environmental studies using a data assimilation approach," *GISci. Remote Sens.*, vol. 50, no. 5, pp. 500–514, 2013.

[4] B. Chen et al., "Changes in vegetation photosynthetic activity trends across the Asia–Pacific region over the last three decades," *Remote Sens. Environ.*, vol. 144, pp. 28–41, 2014.

[5] S. Piao et al., "Plant phenology and global climate change: Current progresses and challenges," *Glob. Change Biol.*, vol. 25, no. 6, pp. 1922–1940, 2019.

[6] X. Zhang et al., "Monitoring vegetation phenology using MODIS," *Remote Sens. Environ.*, vol. 84, no. 3, pp. 471–475, 2003.

[7] R. Liu, R. Shang, Y. Liu, and X. Lu, "Global evaluation of gap-filling approaches for seasonal NDVI with considering vegetation growth trajectory, protection of key point, noise resistance and curve stability," *Remote Sens. Environ.*, vol. 189, pp. 164–179, 2017.

[8] X. Tang, E. L. Bullock, P. Olofsson, S. Estel, and C. E. Woodcock, "Near real-time monitoring of tropical forest disturbance: New algorithms and assessment framework," *Remote Sens. Environ.*, vol. 224, pp. 202–218, 2019.

[9] A. Kawabata, K. Ichii, and Y. Yamaguchi, "Global monitoring of interannual changes in vegetation activities using NDVI and its relationships to temperature and precipitation," *Int. J. Remote Sens.*, vol. 22, no. 7, pp. 1377–1382, 2001.

[10] J. Chen et al., "A simple method for reconstructing a high-quality NDVI time-series data set based on the Savitzky–Golay filter," *Remote Sens. Environ.*, vol. 91, no. 3/4, pp. 332–344, 2004.

[11] P. M. Atkinson, C. Jeganathan, J. Dash, and C. Atzberger, "Inter-comparison of four models for smoothing satellite sensor time-series data to estimate vegetation phenology," *Remote Sens. Environ.*, vol. 123, pp. 400–417, 2012.

[12] J. J. Walker, K. M. De Beurs, R. H. Wynne, and F. Gao, "Evaluation of Landsat and MODIS data fusion products for analysis of dryland forest phenology," *Remote Sens. Environ.*, vol. 117, pp. 381–393, 2012.

[13] K. J. Wessels, F. Van Den Bergh, and R. J. Scholes, "Limits to detectability of land degradation by trend analysis of vegetation index data," *Remote Sens. Environ.*, vol. 125, pp. 10–22, 2012.

[14] L. Jiang, Y. Liu, S. Wu, and C. Yang, "Analyzing ecological environment change and associated driving factors in China based on NDVI time series data," *Ecol. Indicators*, vol. 129, 2021, Art. no. 107933.

[15] Y. Ju and G. Bohrer, "Classification of wetland vegetation based on NDVI time series from the HLS dataset," *Remote Sens.*, vol. 14, no. 9, 2022, Art. no. 2107.

[16] H. Gim et al., "Improved mapping and change detection of the start of the crop growing season in the US corn belt from long-term AVHRR NDVI," *Agricultural Forest Meteorol.*, vol. 294, 2020, Art. no. 108143.

[17] W. Ni et al., "Seasonal effects on aboveground biomass estimation in mountainous deciduous forests using ZY-3 stereoscopic imagery," *Remote Sens. Environ.*, vol. 289, 2023, Art. no. 113520.

[18] R. De Jong, S. de Bruin, A. de Wit, M. E. Schaepman, and D. L. Dent, "Analysis of monotonic greening and browning trends from global NDVI time-series," *Remote Sens. Environ.*, vol. 115, no. 2, pp. 692–702, 2011.

[19] X. Zhu, G. Xiao, D. Zhang, and L. Guo, "Mapping abandoned farmland in China using time series MODIS NDVI," *Sci. Total Environ.*, vol. 755, 2021, Art. no. 142651.

[20] C. Dong, C. C. Loy, K. He, and X. Tang, "Image super-resolution using deep convolutional networks," *IEEE Trans. Pattern Anal. Mach. Intell.*, vol. 38, no. 2, pp. 295–307, Feb. 2016.

[21] S. M. A. Bashir, Y. Wang, M. Khan, and Y. Niu, "A comprehensive review of deep learning-based single image super-resolution," *PeerJ. Comput. Sci.*, vol. 7, 2021, Art. no. e621.

[22] T. Tong, G. Li, X. Liu, and Q. Gao, "Image super-resolution using dense skip connections," in *Proc. IEEE Int. Conf. Comput. Vis.*, 2017, pp. 4799–4807.

[23] B. Lim, S. Son, H. Kim, S. Nah, and K. M. Lee, "Enhanced deep residual networks for single image super-resolution," in *Proc. IEEE Conf. Comput. Vis. Pattern Recognit. Workshops*, 2017, pp. 136–144.

[24] L. Hassan-Esfahani, A. M. Ebtehaj, A. Torres-Rua, and M. Mckee, "Spatial scale gap filling using an unmanned aerial system: A statistical downscaling method for applications in precision agriculture," *Sensors*, vol. 17, no. 9, 2017, Art. no. 2106.

[25] R. Nomura and K. Oki, "Downscaling of MODIS NDVI by using a convolutional neural network-based model with higher resolution SAR data," *Remote Sens.*, vol. 13, no. 4, 2021, Art. no. 732.

[26] J. Talreja, S. Aramvith, and T. Onoye, "DANS: Deep attention network for single image super-resolution," *IEEE Access*, vol. 11, pp. 84379–84397, 2023.

[27] T. I. Ibrahim, S. Al-Maliki, O. Salameh, I. Waltner, and Z. Vekerdy, "Improving LST downscaling quality on regional and field-scale by parameterizing the DisTrad method," *ISPRS Int. J. Geo-Inf.*, vol. 11, no. 6, 2022, Art. no. 327.

[28] M. Rhif, A. B. Abbes, B. Martínez, I. R. Farah, and M. A. Gilabert, "Optimal selection of wavelet transform parameters for spatio-temporal analysis based on non-stationary NDVI MODIS time series in mediterranean region," *ISPRS J. Photogrammetry Remote Sens.*, vol. 193, pp. 216–233, 2022.

[29] C. Dong, C. C. Loy, and X. Tang, "Accelerating the super-resolution convolutional neural network," in *Proc. 14th Eur. Conf. Comput. Vis.*, 2016, pp. 391–407.

[30] W. Shi et al., "Real-time single image and video super-resolution using an efficient sub-pixel convolutional neural network," in *Proc. IEEE Conf. Comput. Vis. Pattern Recognit.*, 2016, pp. 1874–1883.

[31] H. Luan, "Establishing the downscaling and spatiotemporal scale conversion models of NDVI based on fractal methodology," in *Fractal Analysis-Selected Examples*. London, U.K.: IntechOpen, 2020.

[32] X. Mao, C. Shen, and Y. Yang, "Image restoration using very deep convolutional encoder-decoder networks with symmetric skip connections," in *Proc. 30th Int. Conf. Neural Inf. Process. Syst.*, Barcelona, Spain, 2016, pp. 2810–2818.

[33] K. He, X. Zhang, S. Ren, and J. Sun, "Deep residual learning for image recognition," in *Proc. IEEE Conf. Comput. Vis. Pattern Recognit.*, 2016, pp. 770–778.

[34] M. Sdraka et al., "Deep learning for downscaling remote sensing images: Fusion and super-resolution," *IEEE Geosci. Remote Sens. Mag.*, vol. 10, no. 3, pp. 202–255, Sep. 2022.

[35] D. C. Lepcha, B. Goyal, A. Dogra, and V. Goyal, "Image super-resolution: A comprehensive review, recent trends, challenges and applications," *Inf. Fusion*, vol. 91, pp. 230–260, 2023.

[36] Y. Zhang, Y. Tian, Y. Kong, B. Zhong, and Y. Fu, "Residual dense network for image super-resolution," in *Proc. IEEE Conf. Comput. Vis. Pattern Recognit.*, 2018, pp. 2472–2481.

[37] J. Kim, J. K. Lee, and K. M. Lee, "Accurate image super-resolution using very deep convolutional networks," in *Proc. IEEE Conf. Comput. Vis. Pattern Recognit.*, 2016, pp. 1646–1654.

[38] Y. Xiao, Y. Wang, Q. Yuan, J. He, and L. Zhang, "Generating a long-term (2003−2020) hourly 0.25° global PM2. 5 dataset via spatiotemporal downscaling of CAMS with deep learning (DeepCAMS)," *Sci. Total Environ.*, vol. 848, 2022, Art. no. 157747.

[39] T. Yu, R. Yang, Y. Huang, J. Gao, and Q. Kuang, "Terrain-guided flatten memory network for deep spatial wind downscaling," *IEEE J. Sel. Topics Appl. Earth Observ. Remote Sens.*, vol. 15, pp. 9468–9481, Oct. 2022.

[40] T. Vandal et al., "DeepSD: Generating high resolution climate change projections through single image super-resolution," in *Proc. 23rd Assoc. Comput. Mach. SIGKDD Int. Conf. Knowl. Discov. Data Mining*, 2017, pp. 1663–1672.

[41] Y. Sha, D. J. Gagne, G. West, and R. Stull, "Deep-learning-based gridded downscaling of surface meteorological variables in complex terrain. Part I: Daily maximum and minimum 2-m temperature," *J. Appl. Meteorol. Climatol.*, vol. 59, no. 12, pp. 2057–2073, 2020.

[42] Z. Ma et al., "A global 250-m downscaled NDVI product from 1982 to 2018," *Remote Sens.*, vol. 14, no. 15, 2022, Art. no. 3639.

[43] J. Fan et al., "The spatio-temporal evolution characteristics of the vegetation NDVI in the Northern slope of the Tianshan mountains at different spatial scales," *Sustainability*, vol. 15, no. 8, 2023, Art. no. 6642.

[44] X. Li, X. He, and X. Pan, "Application of Gaofen-6 images in the downscaling of land surface temperatures," *Remote Sens.*, vol. 14, no. 10, 2022, Art. no. 2307.

[45] W. Jing, Y. Yang, X. Yue, and X. Zhao, "A comparison of different regression algorithms for downscaling monthly satellite-based precipitation over North China," *Remote Sens.*, vol. 8, no. 10, 2016, Art. no. 835.

[46] C. Chen, B. Hu, and Y. Li, "Easy-to-use spatial random-forest-based downscaling-calibration method for producing precipitation data with high resolution and high accuracy," *Hydrol. Earth Syst. Sci.*, vol. 25, no. 11, pp. 5667–5682, 2021.

[47] K. He, W. Zhao, L. Brocca, and P. Quintana-Seguí, "SMPD: A soil moisture-based precipitation downscaling method for high-resolution daily satellite precipitation estimation," *Hydrol. Earth Syst. Sci.*, vol. 27, no. 1, pp. 169–190, 2023.

[48] C. Yoo et al., "Downscaling MODIS nighttime land surface temperatures in urban areas using ASTER thermal data through local linear forest," *Int. J. Appl. Earth Observ. Geoinf.*, vol. 110, 2022, Art. no. 102827, doi: 10.1016/j.jag.2022.102827.

[49] X. Xie, A. Li, H. Jin, G. Yin, and J. Bian, "Spatial downscaling of gross primary productivity using topographic and vegetation heterogeneity information: A case study in the Gongga mountain region of China," *Remote Sens.*, vol. 10, no. 4, 2018, Art. no. 647.

[50] Z. Xiao, S. Liang, T. Wang, and Q. Liu, "Reconstruction of satellite-retrieved land-surface reflectance based on temporally-continuous vegetation indices," *Remote Sens.*, vol. 7, no. 8, pp. 9844–9864, 2015.

[51] Z. Xiao, S. Liang, X. Tian, K. Jia, Y. Yao, and B. Jiang, "Reconstruction of long-term temporally continuous NDVI and surface reflectance from AVHRR data," *IEEE J. Sel. Topics Appl. Earth Observ. Remote Sens.*, vol. 10, no. 12, pp. 5551–5568, Dec. 2017.

[52] K. Didan, A. B. Munoz, R. Solano, and A. Huete, "MODIS vegetation index user's guide (Collection 6)," NASA, Washington, DC, USA, 2015.

[53] J. Yang and X. Huang, "The 30 m annual land cover dataset and its dynamics in China from 1990 to 2019," *Earth Syst. Sci. Data*, vol. 13, no. 8, pp. 3907–3925, 2021.
[54] V. Kovalskyy and D. P. Roy, "The global availability of Landsat 5 TM and Landsat 7 ETM+ land surface observations and implications for global 30 m Landsat data product generation," *Remote Sens. Environ.*, vol. 130, pp. 280–293, 2013.
[55] M. A. Wulder et al., "The global Landsat archive: Status, consolidation, and direction," *Remote Sens. Environ.*, vol. 185, pp. 271–283, 2016.
[56] S. Goward et al., "Historical record of Landsat global coverage," *Photogrammetric Eng. Remote Sens.*, vol. 72, no. 10, pp. 1155–1169, 2006.
[57] G. Chander, D. L. Helder, R. Malla, E. Micijevic, and C. J. Mettler, "Consistency of L4 TM absolute calibration with respect to the L5 TM sensor based on near-simultaneous image acquisition," in *Proc. Earth Observ. Syst. XII*, 2007, pp. 161–172.
[58] T. R. Loveland and J. L. Dwyer, "Landsat: Building a strong future," *Remote Sens. Environ.*, vol. 122, pp. 22–29, 2012.
[59] R. Cao et al., "A simple method to improve the quality of NDVI time-series data by integrating spatiotemporal information with the Savitzky–Golay filter," *Remote Sens. Environ.*, vol. 217, pp. 244–257, 2018.
[60] Z. Wang, A. C. Bovik, H. R. Sheikh, and E. P. Simoncelli, "Image quality assessment: From error visibility to structural similarity," *IEEE Trans. Image Process.*, vol. 13, no. 4, pp. 600–612, Apr. 2004.
[61] W. Yang, F. Kogan, W. Guo, and Y. Chen, "A novel re-compositing approach to create continuous and consistent cross-sensor/cross-production global NDVI datasets," *Int. J. Remote Sens.*, vol. 42, no. 16, pp. 6023–6047, 2021.
[62] A. P. Trishchenko, J. Cihlar, and Z. Li, "Effects of spectral response function on surface reflectance and NDVI measured with moderate resolution satellite sensors," *Remote Sens. Environ.*, vol. 81, no. 1, pp. 1–18, 2002.
[63] J. E. Pinzon and C. J. Tucker, "A non-stationary 1981–2012 AVHRR NDVI3g time series," *Remote Sens.*, vol. 6, no. 8, pp. 6929–6960, 2014.
[64] X. Fan and Y. Liu, "A global study of NDVI difference among moderate-resolution satellite sensors," *ISPRS J. Photogrammetry Remote Sens.*, vol. 121, pp. 177–191, 2016.
[65] F. Tian et al., "Evaluating temporal consistency of long-term global NDVI datasets for trend analysis," *Remote Sens. Environ.*, vol. 163, pp. 326–340, 2015.
[66] Y. Sang et al., "Comment on recent global decline of CO_2 fertilization effects on vegetation photosynthesis," *Science*, vol. 373, no. 6562, 2021, Art. no. g4420.
[67] C. Jiang et al., "Inconsistencies of interannual variability and trends in long-term satellite leaf area index products," *Glob. Change Biol.*, vol. 23, no. 10, pp. 4133–4146, 2017.
[68] S. O. Los, "Estimation of the ratio of sensor degradation between NOAA AVHRR channels 1 and 2 from monthly NDVI composites," *IEEE Trans. Geosci. Remote Sens.*, vol. 36, no. 1, pp. 206–213, Jan. 1998.
[69] K. M. de Beurs and G. M. Henebry, "Trend analysis of the Pathfinder AVHRR land (PAL) NDVI data for the deserts of Central Asia," *IEEE Geosci. Remote Sens. Lett.*, vol. 1, no. 4, pp. 282–286, Oct. 2004.
[70] Z. Wang et al., "Large discrepancies of global greening: Indication of multi-source remote sensing data," *Glob. Ecol. Conservation*, vol. 34, 2022, Art. no. e2016.
[71] Z. Zhu et al., "Global data sets of vegetation leaf area index (LAI) 3g and fraction of photosynthetically active radiation (FPAR) 3g derived from global inventory modeling and mapping studies (GIMMS) normalized difference vegetation index (NDVI3g) for the period 1981 to 2011," *Remote Sens.*, vol. 5, no. 2, pp. 927–948, 2013.
[72] X. Zhang et al., "Exploration of scaling effects on coarse resolution land surface phenology," *Remote Sens. Environ.*, vol. 190, pp. 318–330, 2017.
[73] X. Chen, D. Wang, J. Chen, C. Wang, and M. Shen, "The mixed pixel effect in land surface phenology: A simulation study," *Remote Sens. Environ.*, vol. 211, pp. 338–344, 2018.
[74] L. Liu et al., "How does scale effect influence spring vegetation phenology estimated from satellite-derived vegetation indexes?," *Remote Sens.*, vol. 11, no. 18, 2019, Art. no. 2137.
[75] J. Tian, X. Zhu, J. Wu, M. Shen, and J. Chen, "Coarse-resolution satellite images overestimate urbanization effects on vegetation spring phenology," *Remote Sens.*, vol. 12, no. 1, 2020, Art. no. 117.
[76] W. Chen and G. M. Henebry, "Change of spatial information under rescaling: A case study using multi-resolution image series," *ISPRS J. Photogrammetry Remote Sens.*, vol. 64, no. 6, pp. 592–597, 2009.
[77] D. G. Goodin and G. M. Henebry, "The effect of rescaling on fine spatial resolution NDVI data: A test using multi-resolution aircraft sensor data," *Int. J. Remote Sens.*, vol. 23, no. 18, pp. 3865–3871, 2002.
[78] D. Peng et al., "Investigation of land surface phenology detections in shrublands using multiple scale satellite data," *Remote Sens. Environ.*, vol. 252, 2021, Art. no. 112133.
[79] K. L. Roth, D. A. Roberts, P. E. Dennison, S. H. Peterson, and M. Alonzo, "The impact of spatial resolution on the classification of plant species and functional types within imaging spectrometer data," *Remote Sens. Environ.*, vol. 171, pp. 45–57, 2015.
[80] N. E. Silvero et al., "Soil property maps with satellite images at multiple scales and its impact on management and classification," *Geoderma*, vol. 397, 2021, Art. no. 115089.
[81] A. P. Lopes et al., "Leaf flush drives dry season green-up of the Central Amazon," *Remote Sens. Environ.*, vol. 182, pp. 90–98, 2016.
[82] J. Y. Park et al., "Quantifying leaf phenology of individual trees and species in a tropical forest using unmanned aerial vehicle (UAV) images," *Remote Sens.*, vol. 11, no. 13, 2019, Art. no. 1534.
[83] B. Martínez and M. A. Gilabert, "Vegetation dynamics from NDVI time series analysis using the wavelet transform," *Remote Sens. Environ.*, vol. 113, no. 9, pp. 1823–1842, 2009.
[84] R. K. Paul and P. S. Birthal, "Investigating rainfall trend over India using the wavelet technique," *J. Water Climate Change*, vol. 7, no. 2, pp. 353–364, 2016.
[85] S. M. Vicente-Serrano et al., "Vegetation greening in Spain detected from long term data (1981–2015)," *Int. J. Remote Sens.*, vol. 41, no. 5, pp. 1709–1740, 2020.
[86] M. Rhif, A. Ben Abbes, I. R. Farah, B. Martínez, and Y. Sang, "Wavelet transform application for/in non-stationary time-series analysis: A review," *Appl. Sci.*, vol. 9, no. 7, 2019, Art. no. 1345.
[87] H. Achour, A. Toujani, T. Rzigui, and S. Faïz, "Forest cover in Tunisia before and after the 2011 Tunisian Revolution: A spatial analysis approach," *J. Geovisualization Spatial Anal.*, vol. 2, pp. 1–14, 2018.
[88] A. Dixit and S. Majumdar, "Comparative analysis of Coiflet and Daubechies wavelets using global threshold for image denoising," *Int. J. Adv. Eng. Technol.*, vol. 6, no. 5, 2013, Art. no. 2247.
[89] M. Rhif, A. Ben Abbes, B. Martinez, and I. R. Farah, "An improved trend vegetation analysis for non-stationary NDVI time series based on wavelet transform," *Environ. Sci. Pollut. Res.*, vol. 28, no. 34, pp. 46603–46613, 2021.
[90] A. Hasnaoui and M. Krott, "Forest governance and the Arab spring: A case study of state forests in Tunisia," *Forest Policy Econ.*, vol. 105, pp. 99–111, 2019.
[91] X. Ma et al., "Spatial patterns and temporal dynamics in savanna vegetation phenology across the North Australian Tropical Transect," *Remote Sens. Environ.*, vol. 139, pp. 97–115, 2013.
[92] B. Martínez, S. Sánchez-Ruiz, M. Campos-Taberner, F. J. García-Haro, and M. A. Gilabert, "Exploring ecosystem functioning in Spain with gross and net primary production time series," *Remote Sens.*, vol. 14, no. 6, 2022, Art. no. 1310.
[93] J. M. Costa-Saura, Á. Balaguer-Beser, L. A. Ruiz, J. E. Pardo-Pascual, and J. L. Soriano-Sancho, "Empirical models for spatio-temporal live fuel moisture content estimation in mixed mediterranean vegetation areas using Sentinel-2 indices and meteorological data," *Remote Sens.*, vol. 13, no. 18, 2021, Art. no. 3726.
[94] S. Sánchez-Ruiz, B. Martínez, M. Campos-Taberner, F. J. García-Haro, and M. A. Gilabert, "Análisis de tendencia en la GPP anual sobre la España peninsular," in *Proc. XVIII Congreso Asociación Española Teledetección*, 2019, pp. 24–27.
[95] C. Senf and R. Seidl, "Mapping the forest disturbance regimes of Europe," *Nature Sustain.*, vol. 4, no. 1, pp. 63–70, 2021.
[96] J. Schilling, E. Hertig, Y. Tramblay, and J. Scheffran, "Climate change vulnerability, water resources and social implications in North Africa," *Regional Environ. Change*, vol. 20, pp. 1–12, 2020.
[97] M. F. Allawai and B. A. Ahmed, "Using remote sensing and GIS in measuring vegetation cover change from satellite imagery in Mosul City, North of Iraq," in *Proc. IOP Conf. Ser.: Mater. Sci. Eng.*, 2020, Art. no. 12062.
[98] C. M. Ward, J. Harguess, B. Crabb, and S. Parameswaran, "Image quality assessment for determining efficacy and limitations of super-resolution convolutional neural network (SRCNN)," in *Proc. Appl. Digit. Image Process. XL*, 2017, pp. 19–30.
[99] J. Gu, X. Sun, Y. Zhang, K. Fu, and L. Wang, "Deep residual squeeze and excitation network for remote sensing image super-resolution," *Remote Sens.*, vol. 11, no. 15, 2019, Art. no. 1817.
[100] G. M. Foody and M. K. Arora, "An evaluation of some factors affecting the accuracy of classification by an artificial neural network," *Int. J. Remote Sens.*, vol. 18, no. 4, pp. 799–810, 1997.

Mengmeng Sun received the B.S. degree in surveying and mapping engineering from the Henan Polytechnic University, Jiaozuo, China, in 2016, and the M.E. degree in surveying and mapping engineering from the Henan Polytechnic University, Jiaozuo, China, in 2020. She is currently working toward the Ph.D. degree in geographical information systems with the Faculty of Geographical Science, Beijing Normal University, Beijing, China.

Her research interests include NDVI estimation and spatial downscaling algorithms.

Xiang Zhao received the Ph.D. degree in cartography and geographic information systems from the Beijing Normal University, Beijing, China, in 2006.

From 2008 to 2010, he was a Postdoctoral Fellow with the College of Resources Science and Technology, Beijing Normal University. His research interests include high-performance computing system construction and quantitative remote sensing applications. He also did some research on long time-series remote sensing data trend analysis.

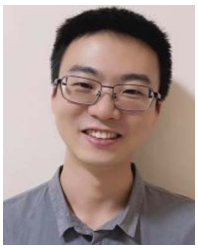

Jiacheng Zhao received the Ph.D. degree in cartography and geographical information systems from the Beijing Normal University, Beijing, China, in 2023.

He has joined the Nanjing University of Information Science and Technology, Nanjing, China, and is currently working on different biophysical traits of trees/crops and their responses to climate change. His research interests include remote sensing, biogeosciences, global change, and landscape modeling.

Naijing Liu received the Ph.D. degree in cartography and geographical information systems from the Beijing Normal University, Beijing, China, in 2023.

He is a currently a joint Postdoc with the POWERCHINA Northwest Engineering Corporation Limited, Xi'an, China and the Beijing Normal University, Beijing, China. His research interests include interactions between renewable energies and local environments.

Siqing Zhao was born in Beijing, China, in March 1999. She received the B.S. degree in geoscience from the Capital Normal University, Beijing, China, in 2021. She is currently working toward the graduate degree in geographical information systems with the Faculty of Geographical Science, Beijing Normal University, Beijing.

Her research interests include ecological remote sensing, conservation priority analysis, and the future direction of ecosystem protection under global changes.

Yinkun Guo received the bachelor's degree in surveying and mapping engineering from the China University of Mining and Technology, Beijing, China, in 2017. He is currently working toward the master's degree in cartography and geographical information systems with the Beijing Normal University, Beijing.

He has recently worked on evaluating the impact of urbanization on ecological quality. His research interests include land cover classification with deep-learning methods, plant diversity, and ecological evaluation in urbanization areas.

Wenxi Shi received the B.S. degree in geography from the Nanjing University of Posts and Telecommunications, Nanjing, China, in 2022.

She is currently studying with the Department of Geographic Sciences, Beijing Normal University, Beijing, China. Her research interests include remote sensing time-series analysis, change detection, and accuracy verification of remote sensing products.

Longping Si received the B.S. degree in computer science and technology from the North China Institute of Aerospace Engineering, Langfang, China, in 2012.

He is currently working with the Beijing Normal University, Beijing, China. His research interests include high-performance computing cluster management and remote sensing product production.